

Exact solution of one dimensional relativistic jet with relativistic equation of state

Raj Kishor Joshi^{1,3}, Indranil Chattopadhyay^{1*}, Dongsu Ryu², Lallan Yadav³

¹*Aryabhata Research Institute of Observational Sciences (ARIES), Manora Peak, Nainital-263002, India.*

²*Department of Physics, School of Natural Science, UNIST, Ulsan 44919, Korea.*

³*Deen Dayal Upadhyaya Gorakhpur University, Gorakhpur, Uttar Pradesh-273009, India*

8 February 2021

ABSTRACT

We study the evolution of one-dimensional relativistic jets, using the exact solution of the Riemann problem for relativistic flows. For this purpose, we solve equations for the ideal special relativistic fluid composed of dissimilar particles in flat space-time and the thermodynamics of fluid is governed by a relativistic equation of state. We obtain the exact solution of jets impinging on denser ambient media. The time variation of the cross-section of the jet-head is modeled and incorporated. We present the initial condition that gives rise to a reverse shock. If the jet-head cross-section increases in time, the jet propagation speed slows down significantly and the reverse-shock may recede opposite to the propagation direction of the jet. We show that the composition of jet and ambient medium can affect the jet solution significantly. For instance, the propagation speed depends on the composition and is maximum for a pair-dominated jet, rather than a pure electron-positron or electron-proton jet. The propagation direction of the reverse-shock may also strongly depend on the composition of the jet.

Key words: hydrodynamics; relativistic processes; shock waves; stars: jets; galaxies: jets

CONTENTS

- 1 Introduction
- 2 Governing equations of relativistic hydrodynamics
 - 2.1 Equation of State (EoS)
 - 2.2 Relativistic shock waves
- 3 Methodology
 - 3.1 Expansion across Jet head
- 4 Results
 - 4.1 Formation of two shock fronts in relativistic jet
 - 4.2 Expanding jet
 - 4.3 Effect of composition parameter
- 5 Discussion and Conclusion
- A Exact solution of Riemann Problem with CR EoS
 - A1 RCS
 - A2 Shock-Contact-Shock (SCS)
 - A3 Solution of relativistic wall shock problem

1 INTRODUCTION

Astrophysical jets were first discovered by Curtis ([Curtis 1918](#)) while studying the M87 galaxy in optical wavelength. With the advent of radio telescopes, the subject of astrophysical jets started to flourish. Now astrophysical jets are studied at least in three wavebands, radio, optical, and X-rays. All these detailed observations revealed that astrophysical jets are quite common and are associated with a variety of objects like AGNs (active galactic nuclei), microquasars, GRBs (gamma-ray bursts), and even YSOs (young stellar objects), albeit in a vastly varied length scales and energetics. Out of these, the jets associated with AGNs, microquasars, and GRBs are relativistic in terms of bulk speed as well as, temperature. After analysing the observations, a general picture emerged that the jets originate from a region very close to the compact objects like black holes residing at the heart of AGNs and microquasars (for example in M87 [Junor et. al. 1999](#); [Doeleman et. al. 2012](#)). From the detailed observations of microquasars, the jet states were found to correlate with the accretion states, suggesting that the jets originated from the accretion discs ([Galo et. al. 2003](#); [Fender et. al. 2010](#); [Rushton et. al. 2010](#)). However, even after the vast improvement in observational facilities, there is no consensus about the composition, formation, and collimation of the jets.

Investigations of astrophysical jets, on one hand, involve the formation problem and on the other, the propagation problem. In this paper, we are interested to study the propa-

* Email: indra@aries.res.in (IC)

gation properties of jets. One of the earliest models for the jet flow was proposed to be a version of the de Laval nozzle by [Blandford & Rees \(1974\)](#). This paper outlined the basic jet structure of a supersonic jet beam far away from the central object. The jet after interaction with the ambient medium, develops a reverse shock in the jet beam, a contact discontinuity, and a forward shock. The separation surface between the jet and the ambient medium is called the contact discontinuity (CD). The forward shock (FS) is the shock transition in the ambient medium as the jet head rams through the ambient medium. And the reverse shock (RS) is in the jet beam. RS and FS are on either side of a CD. [Marscher & Grear \(1985\)](#) associated the flares in the astrophysical jets with traveling shocks along an adiabatic conical jet.

Relativistic jets are studied by solving the equations of relativistic hydrodynamics (RHD). Early attempts involved using explicit finite difference code with monotonic transport ([Wilson 1972](#)). However these kind of codes depended on artificial viscosity techniques to capture shocks. Studies of the interaction of the jet with the ambient medium and the evolution of jet morphology got a tremendous boost with the advent of high resolution shock capturing (or, HRSC) numerical simulation methods ([van Putten 1993](#); [Marti et. al. 1994](#); [Duncan & Hughes 1994](#); [Marti et. al. 1995](#); [Aloy et al. 2003](#); [Walg et al. 2013](#)). HRSC methods solve the fluid equations in the conserved form. The flow variables in the observer frame, also called ‘state vectors’, are updated in time by evaluating the fluxes of these state vectors at the cell surfaces. These fluxes are computed by means of exact or approximate Riemann solvers. RHD codes based on exact Riemann solvers were developed by [Marti & Müller \(1996\)](#); [Wen et. al. \(1997\)](#). There are great variety of numerical schemes available using approximate Riemann solvers. [Balsara \(1994\)](#) developed an approximate Riemann solver using the jump conditions in the shock frame while [Dai & Woodward \(1997\)](#) followed a similar path but by using conditions for oblique shocks. [Eulderink \(1993\)](#); [Eulderink & Mellema \(1995\)](#) extended the Roe-type approximate Riemann solver ([Roe 1981](#)) to RHD. Higher order reconstructions were also proposed ([Marquina et. al. 1992](#); [Dolezal & Wong 1995](#)). More detailed account on the development of HRSC methods can be found in [Marti & Müller \(2003, 2015\)](#).

A global picture of the flow with multiple shocks within a jet has emerged from these simulations.

Most of the simulations were based on the ideal gas equation of state (with a notable exception of [Scheck et. al. 2002](#)) which is a reasonable approximation when the flow remains sub-relativistic or extremely relativistic, but the jets travel over a long distance and the jet material can go through a transition from the relativistic to the non-relativistic regime and vice versa. It may be noted that a flow can be called relativistic on the account when its bulk velocity $v \sim c$ (where c is the speed of light in vacuum) or if the thermal energy of the flow kT (k is the Boltzmann constant and T is the temperature) is of the order, or greater than the rest mass energy of the gas particles. Assuming relativistic Maxwell-Boltzmann distribution of particles, the energy density of the flow or the equation of state (EoS) of the fluid, was computed independently by various authors ([Chandrasekhar 1938](#); [Synge 1957](#); [Cox & Giuli 1968](#)), which were a combination of modified Bessel’s function of various kinds. This EoS is relativistically perfect and is abbreviated

as RP. By using the recurrence relation, [Vyas et al. \(2015\)](#) showed the equivalence between the different forms of the RP EoS, obtained by various authors mentioned above. One of the features of such relativistic EoS is that one need not specify any adiabatic index to describe the thermodynamics of the fluid. The adiabatic index is a function of temperature and can be automatically obtained if the temperature is known. Although it is possible to implement the RP in numerical simulation codes, but the presence of the modified Bessel function makes it computationally expensive ([Falle & Komissarov 1996](#)). Additionally, [Taub \(1948\)](#) in his seminal paper of relativistic shock adiabat, also obtained a relation between thermodynamic variables of the fluid in the form of a fundamental inequality which any EoS of relativistic fluid should obey, and is called the ‘Taub’s inequality’ or TI. Any approximate EoS, apart from being a very good fit of RP, should simultaneously obey TI too. To circumvent the problem of using RP at an extra computational cost, a number of approximate relativistic EoS were proposed by various authors ([Mignone et. al. 2005](#); [Ryu et. al. 2006](#)). The EoS used by [Mignone et. al.](#) is actually the lower limit of TI. On the other hand, [Ryu et. al. \(2006\)](#) proposed a more accurate approximate EoS, and yet the energy density or the enthalpy of the fluid is an algebraic function of pressure and mass density. One can compute the adiabatic index (Γ) from this EoS and it gave correct asymptotic values at non-relativistic and relativistic temperatures. [Chattopadhyay & Ryu \(2009\)](#), extended the EoS of [Ryu et. al.](#) for the fluids composed of dissimilar particles and the EoS is abbreviated as CR. In this work, we use CR EoS which has been applied to a variety of astrophysical scenarios ([Chattopadhyay & Chakrabarti 2011](#); [Cielo et. al. 2014](#); [Chattopadhyay & Kumar 2016](#); [Vyas & Chattopadhyay 2018](#); [Sarkar & Chattopadhyay 2019](#); [Sarkar, Chattopadhyay, Laurent 2020](#); [Singh & Chattopadhyay 2019](#); [Dihingia et al. 2018](#)).

An astrophysical jet is a relativistic beam plying through an ambient medium. The beam of the jet, because it is relativistic should be less dense than the surrounding medium. Therefore, the propagation of jets through a medium is essentially the time evolution of an initial discontinuity between two states of a fluid which on one side is lighter and fast, and denser and static on the other side. There might be a pressure/composition jump across the initial discontinuity or the pressure/composition may also be uniform. Such an initial value problem is generally known as the Riemann problem. Depending on the physical condition of the initial discontinuity, a Riemann problem might evolve into a shock-tube problem, oppositely moving shock waves or oppositely moving rarefaction waves, a wall shock, etc. In the Newtonian regime, solutions of the Riemann problem played an important role in testing several hydrodynamic codes ([Sod 1978](#)). Most of the modern hydrodynamic codes in the Newtonian regime are based on exact or approximate Riemann problem solutions ([LeVeque 1992](#)), such that building a better Riemann solver (exact or approximate), has become a very important field of research ([Toro 1997](#)). Codes developed based on the above techniques and in the Newtonian regime, have been used extensively to study diverse fields like the formation of stars in the galactic plane ([Kim & Ostriker 2001](#)), supernovae ejecta propagation ([Arnett et. al. 1989](#)), cosmolog-

ical simulations (Ryu et al. 1993), accretion discs (Ryu et al. 1995; Ryu et al. 1997), etc.

In 1994, Marti & Müller derived analytical solutions of the Riemann problem for special relativistic fluid, but only for the flow with velocity component normal to the initial discontinuity. This paper helped to test and even develop various numerical simulation codes for relativistic fluid (also see Lora-Clavijo et al. 2013). However, because of the existence of the upper limit of the fluid velocity, the velocity components are not entirely independent of each other. As a result, the form of the eigenvalues of a flow with normal and tangential velocity components with respect to the discontinuity, are different from that of a flow with only a normal velocity component. Pons et al. (2000) generalized the analytical Riemann problem of relativistic fluid obtained by Marti & Müller for arbitrary tangential velocity components. The Riemann problem associated with relativistic jets is characterised by an FS, a CD or the jet head, and the RS somewhere in the jet beam. The solution of Riemann problem with a fixed adiabatic index EoS is relatively easier, but we will discuss later that such a solution is non-trivial with a relativistic EoS like CR. Although, exact solutions of the Riemann problem are generally used to test simulation codes, but these problems resemble astrophysical scenarios, so if judiciously used, exact solutions of the Riemann problem can be used to study astrophysical problems as well (Harpole & Hawke 2019).

In this paper, we solve the Riemann problem associated with a relativistic jet. The thermodynamics of the flow is described by CR EoS. All the basic features of the relativistic jet are discussed considering an electron-proton flow. In this paper, we would like to find the necessary condition for which the initial discontinuity develops into two shocks, the reverse shock in the jet beam and a forward shock in the ambient medium ahead of the jet head. We would like to investigate how the expanding jet-head cross-section affects the evolution of the jet. We also study the effect of jet fluid composition on the overall jet evolution. We investigate the effect of the composition of the jet beam on jet evolution, while keeping the ambient composition same. We compared the effect of the ambient medium composition on jet evolution, while keeping the jet composition same. For the sake of completeness, we have given a short account of the solution of a relativistic shock tube problem and wall-shock problem in the Appendix. We also compared the exact solution of the wall-shock with the relativistic TVD simulation code (Ryu et al. 2006; Chattopadhyay et al. 2013) in the Appendix.

In section 2, we present the governing equations. In section 2.1, we describe the CR EoS for fluid composed of dissimilar particles. In section 2.2, the structure of relativistic shocks is described. We discuss the methodology to obtain the solution in section 3. In section 4.1, we derive the condition for the formation of two shocks of a jet. In section 4.2, we discuss the effect of an expanding cross-section of the jet head, on the structure of the jet. In sections 4.3, 4.3.1, 4.3.2, we discuss the effect of fluid composition on the evolution of jets. And finally, in section 5 we discuss the highlights and summarize the results. In addition, we also present exact solutions of two types of relativistic Riemann problem, one is the shock-contact-rarefaction fan problem or a shock-tube problem and two, shock-contact-shock with CR EoS in Appendix A.

2 GOVERNING EQUATIONS OF RELATIVISTIC HYDRODYNAMICS

We study ideal, relativistic fluid in flat space-time, and the energy-momentum tensor of such a fluid is given by;

$$T^{\mu\nu} = \rho h u^\mu u^\nu + p \eta^{\mu\nu}, \quad (1)$$

where ρ , p , and h are the rest-mass density, local pressure, and the specific enthalpy of the fluid, respectively. We follow the convention where the Greek indices represent space-time components of the vectors and tensors. Contravariant components of the four-velocity are represented by u^μ and $\eta^{\mu\nu}$ are the components of Minkowski metric tensor in the Cartesian coordinates.

$$\eta^{\mu\nu} = \text{diag}(-1, 1, 1, 1) \quad (2)$$

Four-velocity of the fluid satisfies the normalization condition i.e. ¹

$$u^\mu u_\mu = -1 \quad (3)$$

The conservation of mass flux and energy-momentum gives us the relativistic fluid equations of motion.

$$(\rho u^\nu)_{,\nu} = 0 \quad (4)$$

$$T^{\mu\nu}_{,\nu} = 0 \quad (5)$$

Using the normalization condition (3) we can write four-velocity as

$$u^\mu = \gamma(1, v^x, v^y, v^z) \quad [v_i = v^i \text{ components of three velocity}] \quad (6)$$

where γ is the Lorentz factor

$$\gamma = (1 - v^2)^{-\frac{1}{2}} \quad (7)$$

and

$$v^2 = (v^x)^2 + (v^y)^2 + (v^z)^2 \quad (8)$$

In Minkowski space-time, the equations of relativistic hydrodynamics can be written in conservative form

$$\partial_t \mathbf{U} + \partial_i \mathbf{F}^{(i)} = 0 \quad (9)$$

Where \mathbf{U} and $\mathbf{F}^{(i)}$ ($i \equiv x, y, z$) are the vectors and fluxes of the conserved variables, respectively.

$$\mathbf{U} = (D, M^x, M^y, M^z, E)^T \quad (10)$$

$$\mathbf{F}^{(i)} = (Dv^i, M^x v^i + p \delta^{xi}, M^y v^i + p \delta^{yi}, M^z v^i + p \delta^{zi}, (E+p)v^i)^T \quad (11)$$

where conserved variables D , M^i , and E denote the mass density, momentum density, and energy density, respectively.

¹ Throughout this paper we will use unit system where speed of light c is set to unity, unless mentioned otherwise

These conserved variables can also be written in terms of primitive variables,

$$\begin{aligned} D &= \rho\gamma \\ M^i &= \rho h\gamma^2 v^i \\ E &= \rho h\gamma^2 - p \end{aligned} \quad (12)$$

The equation of state (EoS) is used to close the set of equations (9). The EoS can be written in form

$$e = e(p, \rho) \quad (13)$$

where e is the energy density in the local frame.

The set of equations of motion (4, 5 or 9) are hyperbolic in nature and admits five real eigenvalues. Three of which are degenerate and are the entropy mode, while the first and the last one are non-degenerate and are the acoustic modes. The eigenvalues are:

$$\begin{aligned} \beta_1 &= \frac{v^x(1-c_s^2)-c_s\sqrt{(1-v^2)[1-v^2c_s^2-(v^x)^2(1-c_s^2)]}}{1-v^2c_s^2} \\ \beta_2 &= v^x \\ \beta_3 &= v^x \\ \beta_4 &= v^x \\ \beta_5 &= \frac{v^x(1-c_s^2)+c_s\sqrt{(1-v^2)[1-v^2c_s^2-(v^x)^2(1-c_s^2)]}}{1-v^2c_s^2} \end{aligned} \quad (14)$$

Here $c_s = \sqrt{(\partial p/\partial e)_s}$ is the adiabatic, relativistic sound speed. The full eigenstructure with right and left eigenvectors for relativistic fluid has also been obtained previously for a general EoS (see Ryu et. al. 2006).

2.1 Equation of State (EoS)

We use CR EoS (Chattopadhyay & Ryu 2009) for the fluids composed of electrons, positrons, and protons. The CR EoS is of the following form

$$e = \sum_i \left(n_i m_i c^2 + p_i \frac{9p_i + 3n_i m_i c^2}{3p_i + 2n_i m_i c^2} \right) \quad (15)$$

In Eq. 15, c is used explicitly. The index i represents the various species that constitute the fluid and c is the speed of light in vacuum. In this paper, we consider the fluid to be composed of electrons, protons, and positrons of various proportion. The above equation can be represented in the unit system where $c = 1$, as,

$$e = \rho f, \quad (16)$$

where,

$$f = 1 + (2 - \xi)\Theta \left[\frac{9\Theta + 6/\tau}{6\Theta + 8/\tau} \right] + \xi\Theta \left[\frac{9\Theta + 6/\eta\tau}{6\Theta + 8/\eta\tau} \right] \quad (17)$$

In the above equations $\rho = \sum_i n_i m_i = n_{e^-} m_{e^-} (2 - \xi + \xi/\eta)$, where $\xi = n_p/n_{e^-}$, $\eta = m_{e^-}/m_p$ and n_{e^-} , n_p , m_{e^-} and m_p are the electron number density, the proton number density, the electron rest mass, and proton rest mass. Moreover, the ratio of the pressure and the local rest energy density of fluid,

is a measure of temperature $\Theta = p/\rho$ and $\tau = 2 - \xi + \xi/\eta$ ². The specific enthalpy is given as

$$h = (e + p)/\rho = f + \Theta; \quad (18)$$

The expression for polytropic index N is given as

$$\begin{aligned} N = \rho \frac{\partial h}{\partial p} - 1 &= \frac{\partial f}{\partial \Theta} = 6 \left[(2 - \xi) \frac{9\Theta^2 + 24\Theta/\tau + 8/\tau^2}{(6\Theta + 8/\tau)^2} \right] \\ &+ 6\xi \left[\frac{9\Theta^2 + 24\Theta/(\eta\tau) + 8/(\eta\tau)^2}{\{6\Theta + 8/(\tau\eta)\}^2} \right] \end{aligned} \quad (19)$$

The polytropic index is not a constant but a function of Θ and ξ . It may be noted that, $N \rightarrow 3$ as $\Theta \gg 1$; while $N \rightarrow 3/2$ as $\Theta \ll 1$, therefore N approaches asymptotic values at very high and low temperatures. It may be noted further that, for $\xi = 0$ (i. e., single species gas), the expression of the polytropic index is exactly same as that was presented in Ryu et. al. (2006). And the adiabatic index Γ is

$$\Gamma = 1 + \frac{1}{N} \quad (20)$$

The variation of adiabatic index Γ with respect to Θ is shown in Fig. (1). The composition of the fluid is marked in the legend, electron-positron or $\xi = 0$ (solid, blue), equal proportion of positrons and protons or $\xi = 0.5$ (dashed, red) and the electron-proton fluid or $\xi = 1.0$ (dashed-dot, black). It is quite clear that $\Theta > 10$ is the ultra-relativistic temperature regime i. e. $\Gamma \rightarrow 4/3$, for a fluid of any composition ξ . On the other hand, $\Theta < 10^{-5}$ is the non-relativistic temperature regime, where $\Gamma \sim 5/3$ for fluid with $\xi > 0$. But for $\xi = 0$, $\Gamma \rightarrow 5/3$ is for $\Theta \lesssim \text{few} \times 10^{-3}$. Clearly, the thermodynamics of the flow depends on both the temperature and the composition ξ of the flow. It may be remembered that the conversion between the absolute temperature T and Θ is given by $T = \tau m_{e^-} \Theta / 2k$. The expression of sound speed starting from the first principle can be written as,

$$c_s^2 = \frac{1}{h} \frac{\partial p}{\partial \rho} = -\frac{\rho}{Nh} \frac{\partial h}{\partial \rho} = \frac{\Gamma\Theta}{h} \quad (21)$$

For non-relativistic temperatures or $\Theta \ll 1$, $h \rightarrow 1$ and $\Gamma \rightarrow 5/3$, sound speed approaches non-relativistic value $c_s \rightarrow \sqrt{5\Theta/3}$. In contrast, for $\Theta \gg 1$, $h \sim 4\Theta$, $\Gamma \sim 4/3$, so $c_s \rightarrow 1/\sqrt{3}$, once again the sound speed achieves asymptotic values for ultra-relativistic and non-relativistic temperature limit.

2.2 Relativistic shock waves

The information about the states on both sides of a shock is obtained by the jump conditions based on the continuity of mass and energy-momentum fluxes. These conditions are known as the Rankine-Hugoniot (RH) conditions. The relativistic version of RH conditions was obtained by Taub (1948). The relativistic RH conditions are given as (also see Pons et. al. 2000)

$$[\rho u^\mu] n_\mu = 0 \quad (22)$$

$$[T^{\mu\nu}] n_\nu = 0 \quad (23)$$

² Although the EoS in equation 16 is exactly same as that in Chattopadhyay & Ryu (2009), but in this paper, τ is included in the definition of Θ and f

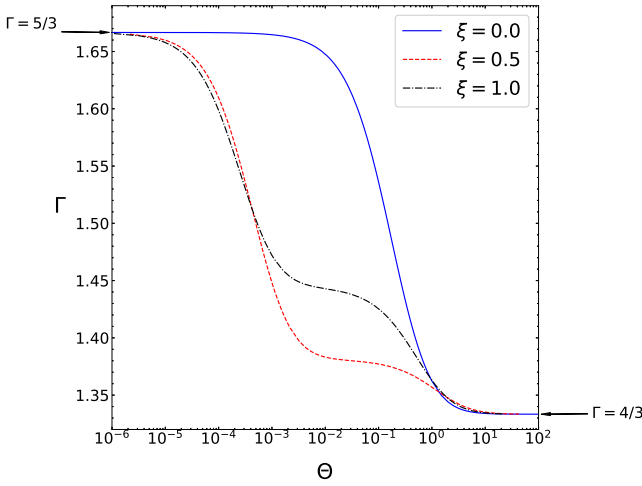


Figure 1. Variation of adiabatic index with Θ for fluids with composition parameter $\xi = 0.0$ (solid blue), $\xi = 0.5$ (red dotted), $\xi = 1.0$ (black dot-dashed).

where n_μ is a unitary normal vector to shock surface Σ and we have used the notation. Here,

$$[F] = F_a - F_b \quad (24)$$

F_a and F_b are the values of the function F on the either sides of the shock surface Σ . Considering Σ to be normal to the x axis and using the unitarity of n_μ , we can write it as

$$n^\mu = \gamma_s(V_s, 1, 0, 0), \quad (25)$$

where V_s is the speed of shock (the speed of surface Σ) and γ_s is the Lorentz factor of the shock.

$$\gamma_s = \frac{1}{\sqrt{1 - V_s^2}} \quad (26)$$

We can introduce the invariant relativistic mass flux j across the shock as

$$j = \gamma_s D_a (V_s - v_a^x) = \gamma_s D_b (V_s - v_b^x) \quad (27)$$

In the above the suffix ‘a’ and ‘b’ denoted the quantities on either side of the shock. The positive (negative) value of j represents the shock propagating to right (left). Multiplying equation (23) with n_μ and using the definition of j (equation 27), we obtain the expression for relativistic mass flux in terms of pressure, enthalpy and density

$$j^2 = -\frac{[p]}{[h/\rho]} \quad (28)$$

We can write the RH conditions equations (22) and (23) in terms of conserved quantities D , M^j , and E as

$$[v^x] = -\frac{j}{\gamma_s} \left[\frac{1}{D} \right] \quad (29)$$

$$[p] = \frac{j}{\gamma_s} \left[\frac{M^x}{D} \right] \quad (30)$$

$$\left[\frac{M^y}{D} \right] = 0 \quad (31)$$

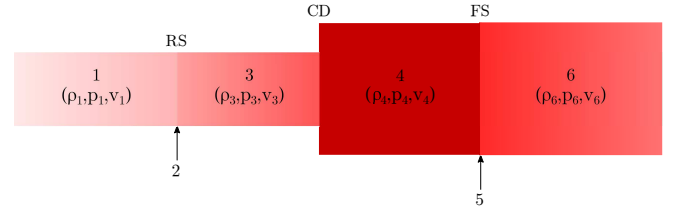


Figure 2. Cartoon diagram of the one dimensional jet (1DJ) structure. The jet is divided into six regions, where region 1 is the original beam of the jet, and region 6 is the original ambient medium. Region 2 is the location of reverse shock (RS), and region 5 is the location of the forward shock (FS). The CD is the location of the jet head (JH). The region 3 is the shocked jet region and region 4 is the shocked ambient medium. Generally the cross-section may vary across every region.

$$\left[\frac{M^z}{D} \right] = 0 \quad (32)$$

$$[v^x p] = \frac{j}{\gamma_s} \left[\frac{E}{D} \right] \quad (33)$$

Equations (31) and (32) imply

$$h\gamma v^{y,z} = \text{constant} \quad (34)$$

$$v_b^{y,z} = h_a \gamma_a v_a^{y,z} \left[\frac{1 - (v_b^x)^2}{h_b^2 + (h_a \gamma_a v_a^t)^2} \right]^{1/2} \quad (35)$$

Where v^t is the absolute value of tangential velocity of the flow.

$$v^t = \sqrt{(v^y)^2 + (v^z)^2} \quad (36)$$

The expression for normal flow velocity v^x is obtained by using equations (29), (30) and (33)

$$v_b^x = \frac{\left(h_a \gamma_a v_a^x + \frac{\gamma_s (p_b - p_a)}{j} \right)}{\left[h_a \gamma_a + (p_b - p_a) \left(\frac{\gamma_s v_a^x}{j} + \frac{1}{\rho_a \gamma_a} \right) \right]} \quad (37)$$

The expression for the shock velocity is obtained using the definition of mass flux

$$V_s^\pm = \frac{\rho_a^2 \gamma_a^2 v_a^x \pm |j| \sqrt{j^2 + \rho_a^2 \gamma_a^2 (1 - (v_a^x)^2)}}{\rho_a^2 \gamma_a^2 + j^2} \quad (38)$$

V_s^+ (V_s^-) corresponds to shock propagating towards right (left).

Multiplying equation (23) first by $(hu_\mu)_a$ and then by $(hu_\mu)_b$ and adding both the expressions results in

$$[h^2] = \left(\frac{h_b}{\rho_b} + \frac{h_a}{\rho_a} \right) [p] \quad (39)$$

Equation (39) is known as Taub adiabat. For the general case Taub adiabat is solved along with the EoS to obtain h_b as a function of p_b .

3 METHODOLOGY

A jet is characterized by low density, high velocity (high v^x), ‘geometrically narrow’ material travelling with relativistic velocity through a denser, colder, static medium. We consider

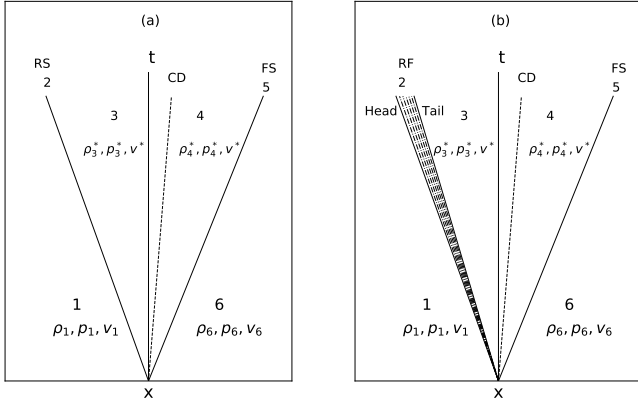


Figure 3. Schematic diagram for: (a) relativistic jet (1DJ) — At $t = 0$, region 1 is the beam of the jet, and region 6 is the ambient medium. The initial discontinuity evolves into a forward shock (FS), and contact discontinuity (CD) and a reverse shock (RS). (b) Shock tube problem — Region 1 and 6 are the initial left and right state and are marked as suffix of the flow variables in the respective regions. The initial discontinuity evolves into a CD flanked by an FS and an RF.

the relativistic jet as the time evolution of a one dimensional, initial discontinuity. The defining distinction being that the initial left state of the fluid is considered as the jet beam, which is lighter than the ambient medium, moving with relativistic speed to the right. The surging jet beam drives a shock on the ambient medium which also moves in the direction of propagation and is called the forward shock (FS). The initial discontinuity evolves with local jet speed and is the jet-head (JH) or contact discontinuity (CD). The CD moves slower than the jet beam and drives a shock in the jet beam and is called the reverse shock (RS).

Therefore, one dimensional jet (1DJ) consists of a forward and a reverse shock separated by a CD. The solution is represented as six regions (see Fig. 2), which are:

- Region 1: It is the initial unperturbed state which is characterised by injection parameters of jet beam, ρ_1 , p_1 and v_1 (i. e., v_1^x).
- Region 2: is a thin surface of RS, which may move in the same direction as FS, but depending on the physical condition may also move in the opposite direction.
- Region 3: It is the region between the RS and the CD. The state is represented as ρ_3^* , p_3^* and v_3^* .
- Region 4: It is the region between CD and FS. There is a density jump across CD and the flow variables in this region are represented as ρ_4^* , p_4^* and v_4^* .
- Region 5 is the surface of FS travelling to the right.
- Region 6: This region corresponds to the ambient medium which has not been influenced by the forward shock wave and the flow variables in this region are represented as ρ_6 , p_6 , & v_6 .

It may be noted that regions 2 and 5 are thin shock surfaces. However, depending on the initial conditions both these surfaces may become rarefaction fan with non-negligible spatial extent (see, Figs. 3a,b for qualitative argument and Figs. 4a-d for a quantitative understanding). Therefore as a part of general approach, these surfaces are called regions. In Fig. (3a), we present the schematic diagram of the time

evolution of these surfaces in 1DJ. Figure (3a) shows that the location of CD, FS, and RS at any time will be on the three straight lines and the values of the flow variables in the six regions will be as mentioned above. It is clear that the time evolution of 1DJ is similar to an initial value problem which is also known as the Riemann problem. Riemann problems are of various kinds, one of the most popular example of one, is the so-called shock-tube (ST) problem. In Fig. (3b), we present the schematic diagram of an ST problem for comparison. It may be remembered that ST too is an initial value problem, however, the initial conditions are such (high pressure/density) that FS and CD forms but instead of an RS, a rarefaction fan (RF) is formed. The RF moves in a direction opposite to FS and CD. The detailed solution procedure for a couple of other Riemann problems is presented in the Appendix. In this paper, we present the solution for 1DJ problem.

The time evolution and solution of the 1DJ problem, depends crucially on the measurement of the post shock velocity. Recalling equation (37) we obtain an expression for $(v_3^x)^*$ in terms of v_1^x for a RS and an expression for $(v_4^x)^*$ in terms of v_6^x for a FS.

$$(v_3^x)^* = \left(h_1 \gamma_1 v_1^x + \frac{\gamma_s (p_* - p_1)}{j} \right) \left(h_1 \gamma_1 + (p_* - p_1) \left(\frac{\gamma_s v_1^x}{j} + \frac{1}{\rho_1 \gamma_1} \right) \right)^{-1} \quad (40)$$

$$(v_4^x)^* = \left(h_6 \gamma_6 v_6^x + \frac{\gamma_s (p_* - p_6)}{j} \right) \left(h_6 \gamma_6 + (p_* - p_6) \left(\frac{\gamma_s v_6^x}{j} + \frac{1}{\rho_6 \gamma_6} \right) \right)^{-1} \quad (41)$$

For equation (40) j is the negative root of equation (28) and for equation (41) it is the positive root of equation (28). The continuity of velocity across JH is the key to obtain the solution of this problem

$$(v_4^x)^* - (v_3^x)^* = 0 \quad (42)$$

Equation (42) is solved for p^* using the iterative root finder and rest of the quantities can be calculated once p^* is obtained. Densities in Region 3 and 4 are obtained from the Taub adiabat for RS and right FS respectively. The $(v_3^x)^* = (v_4^x)^* = (v^x)^*$ is the speed V_j with which the jet-head or CD is propagating.

The continuity of the normal component of velocity follows from the fact that the mass flux across the CD is zero.

$$j = \gamma_j D_a (V_j - v_a^x) = \gamma_j D_b (V_j - v_b^x) = 0 \quad (43)$$

Where V_j is the velocity of jet head or the CD and γ_j is the Lorentz factor of jet head.

3.1 Expansion across Jet head

As the jet expands it can result in discontinuous cross sectional area across the jet head. To obtain the equations that govern the dynamics of the flow when the area across CD/JH

is not same, we use the momentum flux balance across the CD/JH (Mizuta et. al. 2004)

$$A_b [\rho_b h_b \gamma_j^2 (v_b - V_j)^2 + p_b] = A_a [\rho_a h_a \gamma_j^2 (v_a - V_j)^2 + p_a] \quad (44)$$

Using equation (43) with (44) we obtain

$$A_b p_b = A_a p_a \quad (45)$$

And the velocity balance condition across the jet head is given as

$$v_3^* (p_3^*) - v_4^* (p_4^*) = 0 \quad (46)$$

Assuming $p_4^* = p^*$, equation (46) is a transcendental equation for variable p^* , as p_3^* and p_4^* are related by equation (45) as $A_3 p_3^* = A_4 p_4^*$.

The jet kinetic luminosity is related with the jet cross-section

$$L_j = \gamma_1^2 (e + p)_1 v_1 \pi y_1^2, \quad (47)$$

Where quantities with suffix ‘1’ are the jet beam variables where the jet beam velocity $v_1 = v_1^x$, and y_1 is the cross-sectional dimension of the jet beam, so $A_1 = \pi y_1^2$.

4 RESULTS

4.1 Formation of two shock fronts in relativistic jet

The essential condition for the formation of two shock fronts is that the pressure in the intermediate state p^* (refer to Fig 3) should be greater than the pressure in the initial states. Rezzolla & Zanotti (2001) have shown that the intermediate pressure is a function of relative velocities between the initial states so there will be a limiting value of relative velocity for the occurrence of two shock fronts. In this case, we assume the cross-sectional area of the flow to be invariant across all the regions. To obtain the value of limiting velocity we start by assuming the scenario with a left and right shock separated by contact discontinuity. We assume the pressure of jet beam p_1 is greater than the pressure of ambient medium p_6 . Assuming there is an RS, the relative velocity of the pre-shock region (1) and the post-shock region (3) is given by (Rezzolla & Zanotti 2001)

$$v_{13} = \sqrt{\frac{(p^* - p_1)(e_3 - e_1)}{(e_1 + p^*)(e_3 + p_1)}} \quad (48)$$

Similarly, the relative velocity (between region 4 and 6) ahead of FS is given as

$$v_{64} = -\sqrt{\frac{(p^* - p_6)(e_4 - e_6)}{(e_6 + p^*)(e_4 + p_6)}} \quad (49)$$

It may be remembered, $v_3 = v_4 = v^*$ across the CD. Hence the relative velocity of between two initial states is given as

$$(v_{16})_{2S} = \frac{v_{13} - v_{64}}{1 - v_{13}v_{64}} \quad (50)$$

For the limiting case where there exist an RS, the minimum value of pressure in the intermediate region i.e. p^* , is given as

$$p^* = \max(p_1, p_6) = p_1 \quad (51)$$

Hence the limiting value of relative velocity is given as

$$v_{\text{lim}} = \sqrt{\frac{(p_1 - p_6)(e_4 - e_6)}{(e_6 + p_1)(e_4 + p_1)}} \quad (52)$$

As the ambient medium is at rest, therefore the relative velocity between the initial states is $(v_{16})_{2S} = (v_1 - v_6)/(1 - v_1 v_6) = v_1$. For a particular density and pressure configuration, if the injection velocity v_1 is greater than the limiting velocity v_{lim} (see, equation 52), then the injected jet beam evolves with an FS and an RS, otherwise, it evolves as a standard shock-tube problem with an FS and an RF separated by CD. In Fig. (4a-d) we plot flows with two injection velocities, one with $v_1 < v_{\text{lim}}$ (Fig. 4 a, c) and two with $v_1 > v_{\text{lim}}$ (Fig. 4b, d). The initial parameters are given by

$$p_1 = 100, \rho_1 = 0.1, p_6 = 1.0 \rho_6 = 100, \text{ and } v_6 = 0 \quad (53)$$

The composition parameter of beam and ambient medium is same ($\xi = 1.0$). For the initial parameters (Eq. 53), the threshold injection velocity for the formation of two shock front obtained from Eq. (52) is $v_{\text{lim}} = 0.66$. The threshold level of injection velocity is represented by the dashed line in Figs. (4c & d). Figure (4a & c) show the variation of density and velocity, respectively, as functions of position with beam injection velocity $v_1 = 0.60$. In Figs. (4 b & d) the variation of ρ and v^x are for the case $v_1 = 0.70$. It is clear that the initial discontinuity with the injection $v_1 < v_{\text{lim}}$, evolves into a shock tube problem with an CD flanked by an FS ahead and an RF behind it (Fig. 4a & c). The RF is zoomed in Fig. (4a) for clarity. The CD and FS going to the right while RF to the left. On the other hand, in Fig. (4b & d) $v_1 > v_{\text{lim}}$, the initial discontinuity evolves into a solution which has a CD flanked by an FS and RS. The RS is zoomed in the inset of Fig. (4b).

4.1.1 Pressure matched jet

For a pressure matched jet ($p_1 = p_6$) the threshold value of relative velocity from equation (52) is obtained as

$$v_{\text{lim}} = 0 \quad (54)$$

Hence for any non zero injection velocity v_1 , the pressure matched jet will always evolve as two shock fronts separated by a contact discontinuity. Figure (5) shows the flow variables for a jet beam with initial parameters $\rho_1 = 1.0$, $p_1 = 1.0$, $v_1 = 0.99944$ injected into an ambient medium with $\rho_6 = 100.0$, $p_6 = 1.0$, $v_6 = 0.0$. We have assumed the uniform cross sectional flow for this case.

The density jumps in Fig. (5a), show the positions of RS, CD, and FS (from left to right, respectively). The shocked region of the jet beam is in between CD and RS and the kinetic energy of the jet beam is converted to thermal energy in the post-shock region of RS. This shock heated region contains the most relativistic gas ($\Gamma \sim 4/3$). The shocked ambient medium is in between CD and FS.

4.2 Expanding jet

As the jet ploughs through the ambient medium, the jet head cross-section may expand. To employ the expansion effect we

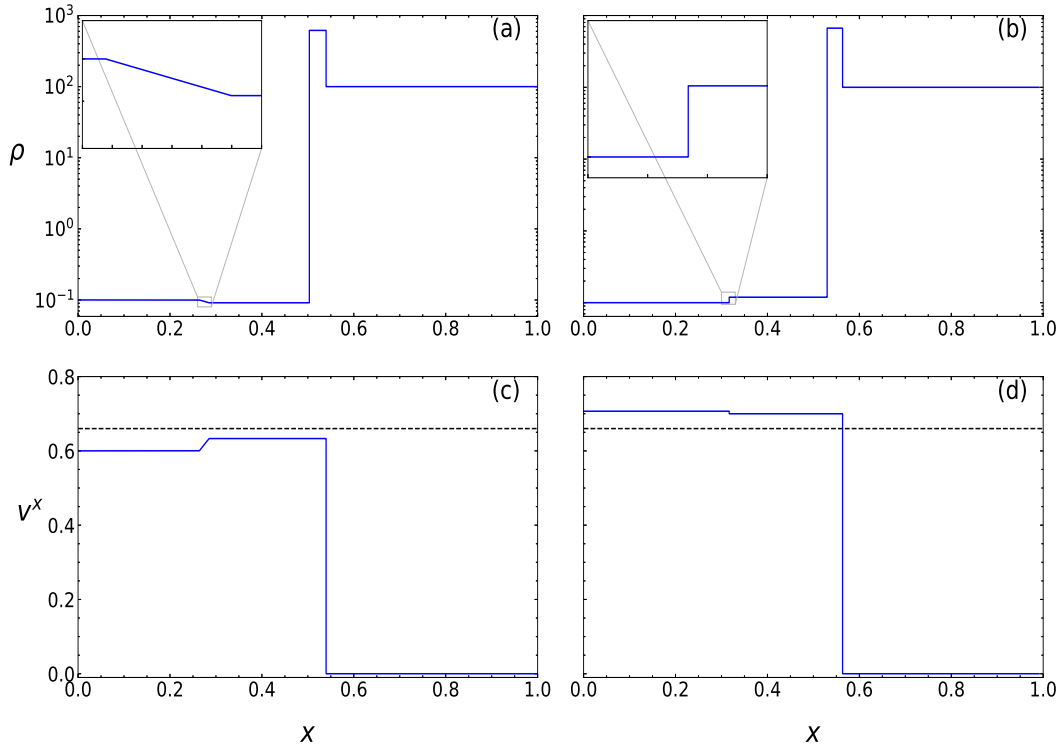


Figure 4. Comparison of a shock-tube (a, c) and 1DJ solution (b, d). The injection velocities are $v_1 = 0.6$ (a, c) and $v_1 = 0.7$ (b, d). Other parameters are $p_1 = 100$, $\rho_1 = 0.1$, $p_6 = 1.0$, $\rho_6 = 100$ and the location of the initial discontinuity is at $x_0 = 0.25$. The plot is at time $t = 0.4$. The composition parameter of injected beam and ambient medium is taken to be $\xi = 1.0$.

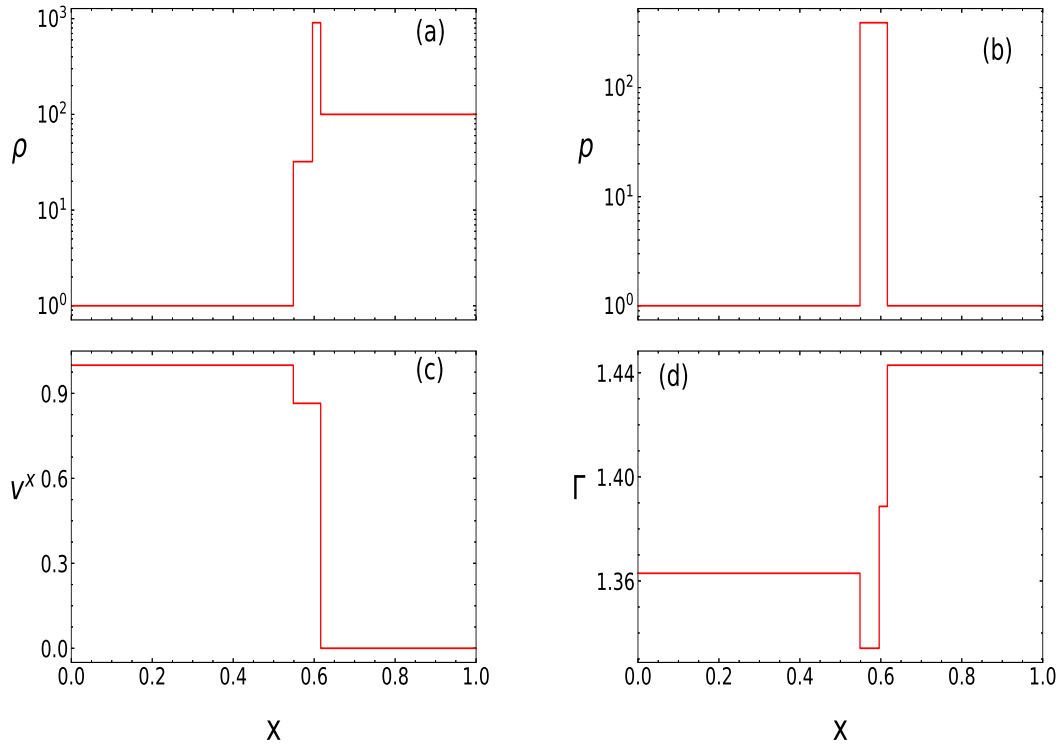


Figure 5. Flow variables (a) ρ , (b) p , (c) v^x and (d) Γ as functions of x at $t = 1.0$ and the fluid composition $\xi = 1.0$. Initial conditions: $\rho_1 = 1.0$, $p_1 = 1.0$, $v_1 = 0.99944$ and $\rho_6 = 100.0$, $p_6 = 1.0$, $v_6 = 0.0$ and the initial discontinuity is at $x_0 = 0.001$.

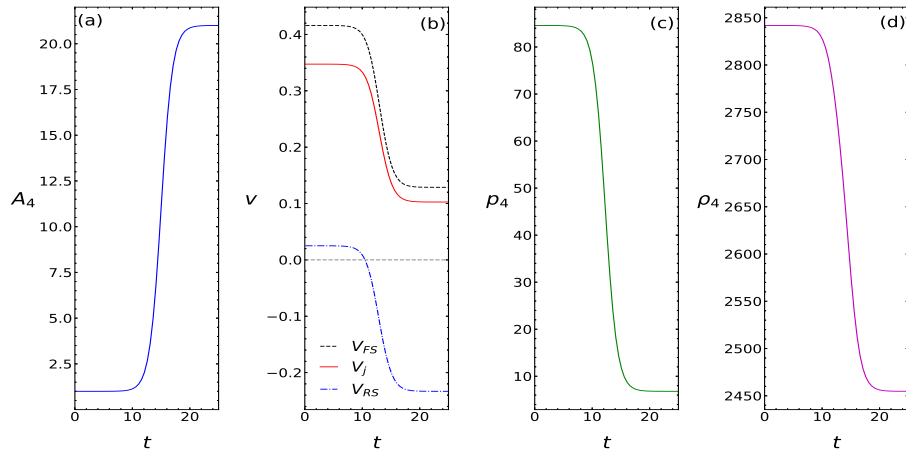


Figure 6. (a) Variation of area ratio across the jet head with respect to time. (b) Variation of the RS, JH and FS velocities as functions of time for an expanding electron-proton jet with injected Lorentz factor 10 and $p_1 = p_6 = 0.1$, $\rho_1 = 1.0$, $\rho_6 = 500.0$ and $x_0 = 0.25$. The variation of pressure and density in region 4 which is the post shock region of FS is shown in panels (c) and (d) respectively.

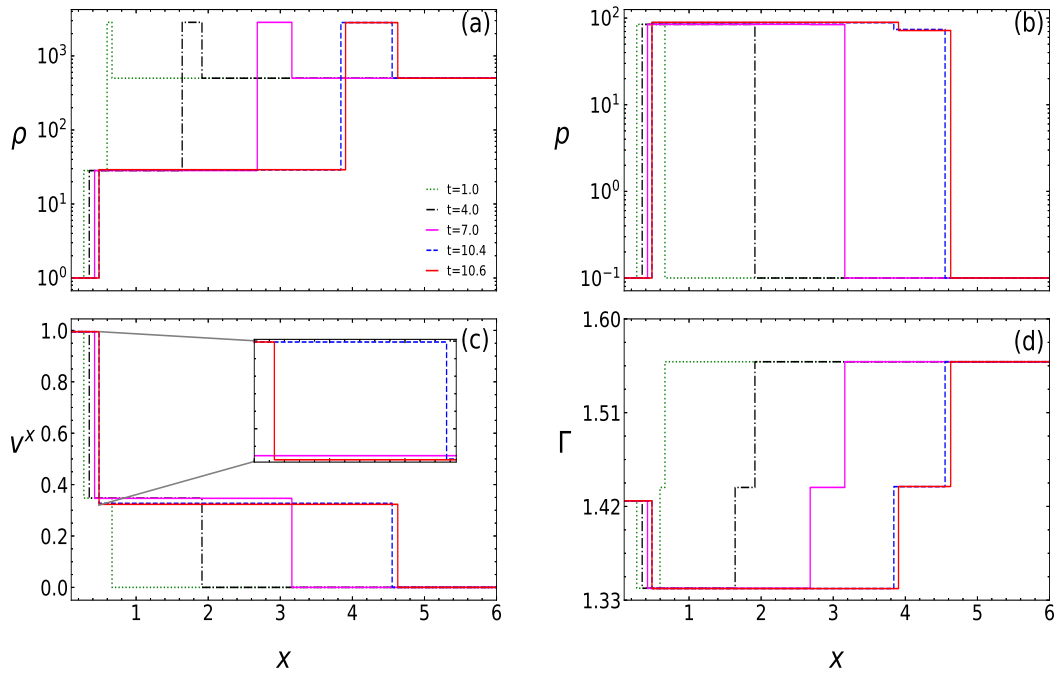


Figure 7. Flow variables $\rho(a)$, $p(b)$, $v^x(c)$ and $\Gamma(d)$ as functions of x at different time for an expanding electron-proton jet. The jet solution are for the same parameters as in Figs. (6).

assume that the area across JH varies in time given by a function

$$A_4 = 1 + C \frac{\exp(t - t_0)}{1 + \exp(t - t_0)} \quad (55)$$

Where C is a constant which sets up and upper limit on A_4 and t_0 limits the onset time for expansion. Figure (6a) is plotted for $C = 20.0$ and $t_0 = 15.0$. From equation 45 one can conclude that across the JH

$$p_3 A_3 = p_4 A_4 \quad (56)$$

Hence the pressure for an expanding jet also exhibits a jump across the CD unlike the Riemann problem where the area across the CD was same. It may however be noted that some

of the additional effects like back flow of jet material and generation of transverse flow components from the region between RS and CD has not been considered for simplicity. Figure (6a) shows the variation of area across JH (A_4) with respect to time t . One may refer to Fig. (2), where we have shown expansion across the jet head, we have assumed the beam area A_1 to be unity and $A_6 = A_4$, also the area across the reverse shock surface is same on both sides ($A_3 = A_1$). In all other sections, we have assumed invariant jet cross-section. In Fig. (6b) we have plotted the propagation velocities V_{RS} (dashed-dotted, blue), V_j (solid, red) and V_{FS} (dashed, black) for a pressure matched electron-proton jet propagating in a homogeneous electron-proton ambient medium. The varia-

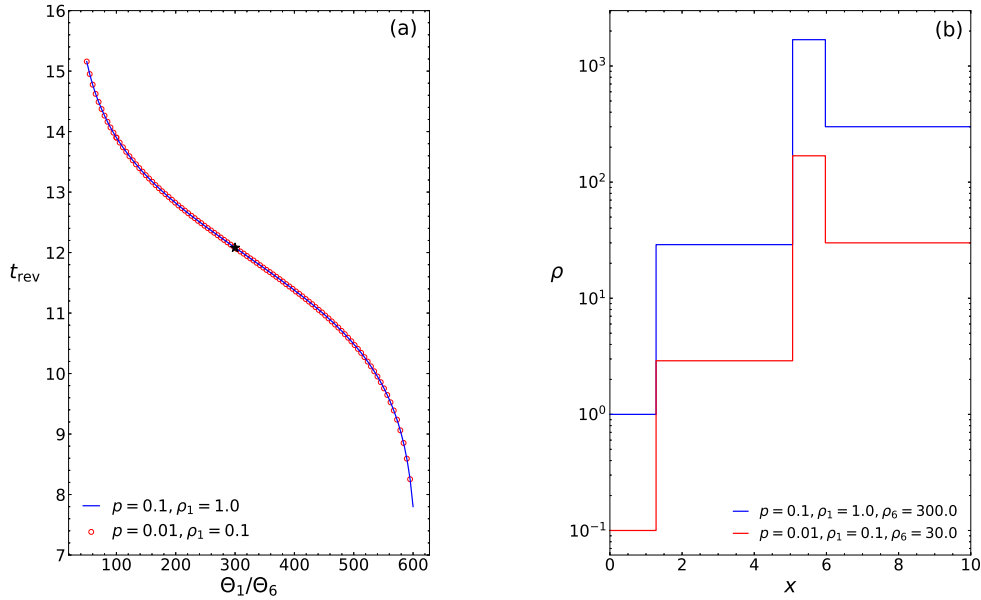


Figure 8. (a) We plot the time t_{rev} taken by RS to move in the opposite direction of JH or CD as a function of Θ_1/Θ_6 . (b) The density profile ρ w.r.t x of the two jets marked by \star ($\equiv t = 12.08$) in panel (a). The injection speed of both the electron-proton ($\xi = 1$) jets $v_1 = 0.995$, but $p_1 = p_6 = p = 0.1$ & $\rho_1 = 1$ for one jet model (solid, blue) and $p_1 = p_6 = p = 0.01$ & $\rho_1 = 0.1$ for the second jet model (open circle, red). ρ_6 for the jets, scale according to the ratio Θ_1/Θ_6 .

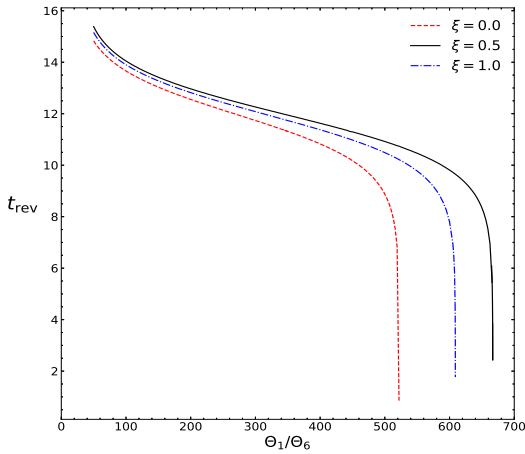


Figure 9. Variation of t_{rev} as a function of Θ_1/Θ_6 for expanding jets with $v_1 = 0.995$, $p_1 = p_6 = 0.1$, $\rho_1 = 1.0$, but for composition $\xi = 0$ (dashed, red), $\xi = 0.5$ (solid, black) and $\xi = 1.0$ (dashed-dotted).

tion of pressure and density in post-shock region of FS (region 4) with respect to time also shown plotted in panel (c) and (d) respectively. Initial discontinuity is at $x_0 = 0.25$ and the initial flow parameters are given as

$$\rho_1 = 1.0, \rho_6 = 500.0, p_1 = p_6 = 0.1, v_1 = 0.995, v_6 = 0.0 \quad (57)$$

Interestingly, as the jet slows down, V_{RS} may become negative or in other words, the RS may start to move backward, as is shown in Fig. (6b), where the RS starts to move backward at $t \sim 10.4$. The corresponding solutions (ρ , p , v^x , & Γ) at different epochs are presented in Figs. (7a-d). The overall jet structure advances forward (to right), however at $t > 10.4$

Fig. (6b) shows that $V_{\text{RS}} < 0$. Therefore Fig. (7c) shows that the RS moves forward from $t = 0 \rightarrow 10.4$, but it moves backward $t = 10.4 \rightarrow 10.6$ (inset shows, solid-red curve for $t = 10.6$ and dashed-dotted-blue for $t = 10.4$). Although, FS and CD continue to move forward. For the initial stages of jet propagation ($t \leq 8.0$), from Fig 6a one can see that the area across the jet head is not changing hence the solution is self similar which is evident from Fig. 7. It may however be noted that, different values of p and initial density contrast ρ_6/ρ_1 would give different values of V_j , V_{FS} and V_{RS} . It is interesting to note that certain physical condition of the environment of the jet may cause the RS to revert back! In Fig. (8a), we plot the time t_{rev} at which the RS starts to move in the reverse direction as a function of initial ratio of Θ_1/Θ_6 , for two electron-proton jets with the same injection Lorentz factor $\gamma_1 = 10$ (i. e., $v_1 = 0.995$) but different pressures and densities of the jet beam $p = 0.1$, & $\rho_1 = 1.0$ (solid, blue) and $p = 0.01$ & $\rho_1 = 0.1$ (open circle, red). Both of the jets are initially pressure matched with the ambient medium. So for a given Θ_1/Θ_6 , initial ambient density ρ_6 scales similarly for both the jets but have different values. For example, the jet with $p = 0.1$ (solid, blue), $\Theta_1/\Theta_6 = 300$ implies $\rho_6 = 300$ while for the jet $p = 0.01$ (open circle, red), the same Θ ratio implies $\rho_6 = 30$. In this figure, we have considered Θ_1/Θ_6 ratio from 50 to 600. The two curves exactly match for the entire range. So even if the pressure and the density of the jets are not similar, the RS reverts back at the same time for a given Θ_1/Θ_6 ratio. It may be noted that, there exists a limiting value of Θ_1/Θ_6 (~ 600 , in this particular case) where the t_{rev} decreases drastically. For any value of Θ_1/Θ_6 greater than this limiting value, the RS will move opposite to the direction of propagation from the start. In Fig. (8b), we compare ρ as a function of x of the jet cases, for parameters corresponding to the black star on the curve in Fig. (8a). Although the density distribution differs between the two jets

being considered here, but the location of RS, CD and FS coincide. Therefore even if the ρ_1 and p are different for the same ratio of the Θ , the jet evolution is exactly similar. It may however be noted that with different p and ρ_1 , the jet kinetic luminosity L_j differs along the curve. In contrast, if the composition parameter is varied for the jet and the beam, t_{rev} is different even if v_1 and Θ_1/Θ_6 are the same. In Fig. (9), we plot the time of reversal of the RS t_{rev} with the ratio Θ_1/Θ_6 for jets with $v_1 = 0.995$, $p_1 = p_6 = 0.1$, $\rho_1 = 1.0$, however for jets for three composition parameter $\xi = 0$ (dashed, red), $\xi = 0.5$ (solid, black) and $\xi = 1.0$ (dash-dotted, blue). Unlike Fig. (8a), the curves for each composition are different. This shows that the evolution of various structures of a jet crucially depend on ξ .

4.3 Effect of composition parameter

The thermal state of the fluid depends upon the ratio T/m (m is the mass of the constituent particles of gas) hence the change in composition parameter will affect the thermal state. To study the effect of the composition parameter on jet morphology we study two scenarios. In the first case, we keep the composition parameter of ambient medium and jet beam same and for the second scenario, we study the case in which the composition of ambient matter differs from the jet composition. To study the effect of composition we have assumed the uniform cross-sectional flow in all the cases.

4.3.1 Same composition parameter for jet and ambient medium

Figure (10) compares the solution snapshots of a relativistic jet at $t = 1.0$ for $\xi = 0.0$ (dashed, red), $\xi = 0.5$ (solid, black) and $\xi = 1.0$ (dash-dotted, blue), with initial parameters

$$\rho_1 = 1.0, \rho_6 = 100.0, p_1 = p_6 = 1.0, v_1 = 0.9988 \quad (58)$$

The density shell between the jet head/contact discontinuity and forward shock is tallest for the jet beam with $\xi = 0.5$ also the adiabatic index is lowest for the same. Hence the jet beam which consists of electron, positron, and proton plasma is hotter than the pure electron-positron jet and the electron-proton jet, provided that the initial injection parameters are same for all. For all the cases, pressure of the shocked material in between CD and FS is considerably higher than the pressure of ambient medium which leads to the formation of over pressured cocoons and these cocoons are responsible for high degree of collimation of the jets (Begelman & Cioffi 1989). The region 4 of the flow with $\xi = 0.5$ is denser than the flow solutions of the other two composition. Even the pressure in region 3 and 4, of the flow with composition parameter $\xi = 0.5$ is greater than that of the flow of other compositions. Hence we expect the flow with $\xi = 0.5$ to be more stable and maintain its collimation over a long-range than the electron-proton jet or electron-positron jet.

4.3.2 Different composition for jet and ambient medium

Figure (11) compares the snapshot of flow variables at $t = 1.0$, for the case when an electron-proton jet ($\xi_1 = 1.0$) is injected into ambient medium with different composition parameters

like $\xi_6 = 0$ (dashed, red), $\xi_6 = 0.5$ (solid, black) and $\xi_6 = 1.0$ (dash-dotted, blue). The initial flow parameters are

$$\rho_1 = 1.0, \rho_6 = 100.0, p_1 = p_6 = 1.0, v_1 = 0.9988 \text{ and } \xi_1 = 1.0 \quad (59)$$

The jet for which the ambient medium is $\xi_6 = 0$, has the widest and tallest high pressure region bounded by FS and RS. It also has the widest high density shell (the region between CD and FS), although the height of the shell is smallest compared to the other two cases. The FS travels with the highest velocity for $\xi_6 = 0$ because of the low resistance offered by the medium. The shock heating is maximum for electron, positron & proton plasma resulting in the lowest adiabatic index in comparison to others. Since the jet beam initial conditions are exactly same in all the three cases, the ambient medium with $\xi_6 = 0$ is the least hot ($\Gamma \sim 5/3$) and therefore offers the least resistance to the jet, which causes the difference in the jet structure as well.

We would now study the effect of composition of a jet beam flowing through the same ambient medium. We consider the cold ambient medium of a static electron-proton fluid. Figure (12) compares the flow variables for jets of different composition traveling in the ambient medium composed of electrons and protons. The composition of the jet beam are $\xi_1 = 0.0$ (dashed, red), 0.5 (solid, black) and 1.0 (dash-dotted). The injected Lorentz factor of the jet is 30 and the initial conditions are,

$$\rho_1 = 1.0, p_1 = 0.1, \rho_6 = 100.0, p_6 = 0.1, v_6 = 0.0 \text{ and } \xi_6 = 1.0 \quad (60)$$

Since the initial condition of the jet is the same, therefore the height of the high density shell between FS and CD have somewhat similar values. Even the height of the high pressure region between RS and FS also is similar. Although pair plasma jets has the lowest ρ and p values. The difference in RS and FS velocities determines the size of post shock region. The post shock region in blazar jets is considered as the flaring region. This region is broadest for electron-positron jet.

4.3.3 Effect of composition on reverse shock

The composition of the jet beam can also affect the direction of propagation of the reverse shock. In Fig. (13) we compare the flow variables of a pressure matched jet beam with Lorentz factor of 10 injected into an electron-proton ambient medium. The initial flow parameters are given as

$$\rho_1 = 1.0, p_1 = 0.1, \rho_6 = 100.0, p_6 = 0.1, v_6 = 0.0 \quad (61)$$

The initial discontinuity was at $x = 0.25$. Figure (13) shows that for pure electron-positron jet beam i.e. $\xi_1 = 0.0$ the reverse shock propagates towards the jet base while a small fraction of protons in the jet beam can revert the direction of reverse shock propagation. In order to drive home this point, we plot the V_{RS} (Fig. 14a), V_j (Fig. 14b) and V_{FS} (Fig. 14c) with the composition parameter of the jet beam ξ_1 . For these flow parameters, the reverse shock moves in the opposite direction for the pair plasma jet. However, V_{RS} increases rapidly with the addition of protons and maximizes for $\xi_1 \sim 0.04$. $V_{\text{RS}} < 0$ again for $\xi_1 \gtrsim 0.24$. The effect of composition on

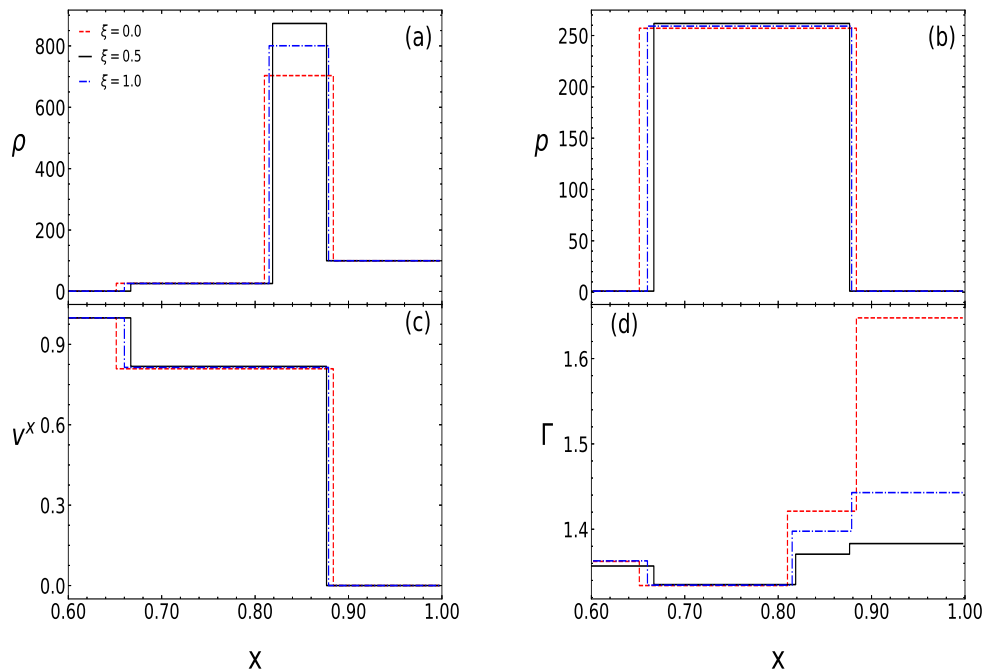


Figure 10. Flow variables $\rho(a)$, $p(b)$, $v^x(c)$ and $\Gamma(d)$ as functions of x at $t = 1.0$. The composition parameter of ambient medium is same as that of jet beam and mentioned in the legends in panel (a). The initial condition is given by $\rho_1 = 1.0$, $\rho_6 = 100.0$, $p_1 = p_6 = 1.0$, $v_1 = 0.9988$ and $x_0 = 0.001$.

various propagation velocities is quite clear, although the effect is more pronounced on V_{RS} . Figure (14b) shows that for these parameters the electron-positron jet is not the fastest jet, instead, a jet with composition $\xi_1 \sim 0.18$ is the fastest.

Finally, in Fig. (15), we plot the injection speed v_1 as a function of Θ_1/Θ_6 for jets of various jet composition $\xi_1 = 0$ (solid, red), $\xi_1 = 0.5$ (dashed, red) and $\xi_1 = 1.0$ (dashed-dotted, red). The lower curve (blue) signifies the locus of injection velocity v_1 for different Θ_1/Θ_6 , below which rarefaction fan (RF) form, and above which reverse shock RS forms but with negative velocity. The upper curve represents the locus of the injection speed above which the RS moves with positive velocity. Assuming the width of the beam y_1 as 1 pc, and the ρ_1 as $10^{-26} \text{ g cm}^{-3}$, we used equation (47) to map the jet luminosity L_j (right label) from the values of v_1 . The limiting velocity v_{lim} does not depend on ξ_1 which is the lower curve and therefore coincides for all ξ_1 . However, the upper curve, which is the limiting injection speed for $V_{RS} > 0$ depends on the composition of the jet.

5 DISCUSSION AND CONCLUSION

In this paper, we obtained the exact solution of time-dependent, one-dimensional relativistic jets plying through external media (or ambient media), by solving equations for the ideal special relativistic fluid composed of dissimilar particles and the thermodynamics of the fluid governed by a relativistic equation of state. The relativistic EoS we used is called the CR EoS, is an approximation of the Chandrasekhar EoS. It is difficult to obtain a general Riemann solution with a general EoS and has been discussed in the introduction. For the sake of completeness, we presented the solution method-

ology and the solutions for three Riemann problems — relativistic shock tube, shock-contact-shock problem and the wall-shock problem in the appendix. The intended impact of this work is firstly to provide exact solutions for numerical simulation codes to compare their results with. But more than that, we studied various properties of the time-dependent relativistic jets, which are in general glossed over. We addressed the issue of the properties of reverse shock. When a reverse shock will form and when will it not. When the reverse shock move in the opposite direction to the jet head and when along with it. We wanted to study the effect of expanding jet-head cross-section on the jet solution. We also wanted to study the effect of the composition of the jet or the ambient medium on the jet solutions and on all these counts we did get interesting results. In the process, we modified the method to solve for jet-like Riemann problem to incorporate the cross-section effect across the jet-head. However, it should be noted that many features of a relativistic jet, like generation of transverse velocity near the jet head, back flow etc are not incorporated in this model for simplicity. Such omission may produce a higher estimate of jet propagation speed, although a suitable modeling of the expanding jet geometry may produce reasonable estimates. The change in cross-section across the jet-head is an approximate attempt to mimic the transverse expansion of the jet and has been discussed in one part of this paper (section 4.2). Such modifications across CD have been attempted earlier (Begelman & Cioffi 1989; Mizuta et. al. 2004).

In this paper, we obtained the condition for the formation of reverse shock and showed that it crucially depends on the injection speed and the initial density contrast between the jet and the ambient medium, although for pressure matched jet that critical injection speed turns out to be zero, in other

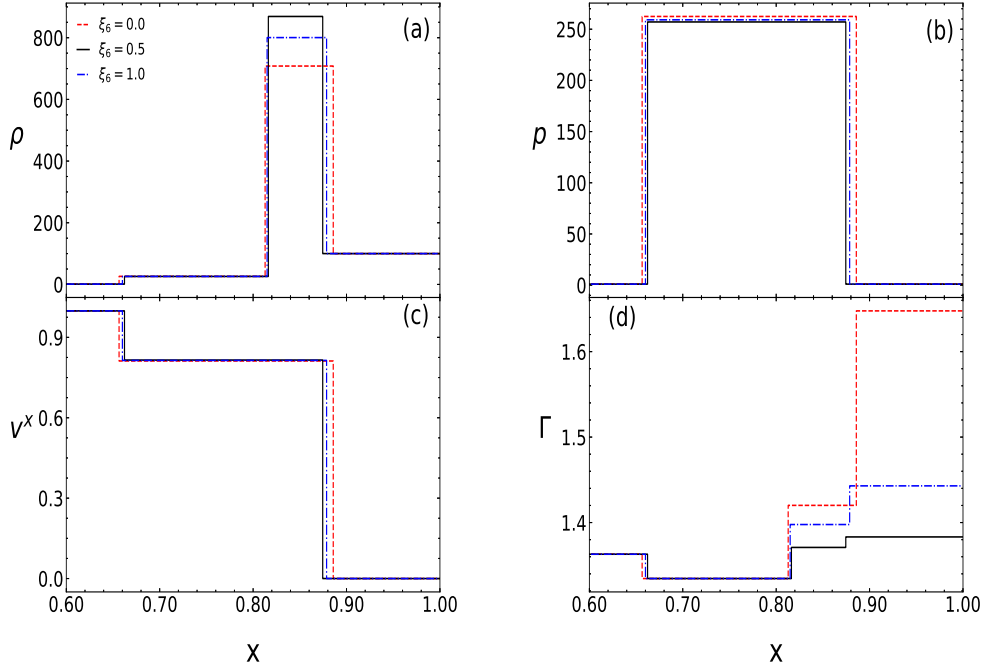


Figure 11. Flow variables (a) ρ , (b) p , (c) v^x and (d) Γ as functions of x at $t = 1.0$ for an ambient medium with composition parameter $\xi_6 = 0.0$ (red dashed), $\xi_6 = 0.5$ (solid black), $\xi_6 = 1.0$ (blue dot-dashed) and $x_0 = 0.001$. The composition parameter of jet beam is taken to be $\xi_1 = 1.0$.

words, in a pressure matched jet a reverse shock will always form. However, if the jet-head cross-section is larger than the beam cross-section, then the reverse shock may travel in the reverse direction. For the particular case of a pressure matched jet which is launched with a Lorentz factor 10 with an initial density contrast of 500, if the cross-section across the jet head remains invariant for some initial time and then expands for some time and settles into a constant value, then we showed that initially RS, CD, and FS moved in the positive direction, after a code time $t \gtrsim 10.4$, RS reversed back. And then as the cross-section settles to a certain uniform value, then the RS also settles to a uniform negative velocity. We also showed that the time of reversal of RS t_{rev} is unique for a given ratio of the initial Θ of the beam and the ambient medium, if the injection speed and composition is same. However, for different values of ξ , t_{rev} will be different even if v_1 and initial Θ ratio is same. Therefore, ξ affects the jet evolution. In general, the propagation speed depends on the beam injection velocities, jet-head cross-section as well as initial density contrast across the surface of separation. We also showed that the composition of the jet also affects the jet structure as it evolves in time, even if all the initial macroscopic fluid variables are same. The composition of the jet plasma affects the jet flow variables like density and pressure and also the propagation velocities like V_{RS} , V_j and V_{FS} too. If jets of different composition flow through an ambient medium of a certain composition, then the jet with less baryons are pushed back. Depending on initial conditions if the jet beam and jet head cross-sections are different then, we showed that for both baryon poor and baryon loaded jets, the reverse shock can go back, even though the jet-head is moving in the positive direction. The composition of the jet not only quantitatively affect the jet flow like different den-

sity, pressure and velocity distribution, but can also produce qualitatively different effects like shocks moving in opposite direction for one composition and shocks moving in the same direction for another composition. We also estimated the injection speed for an initial pressure mismatch jet, for which rarefaction fan (RF) will form instead of the reverse-shock RS and also the upper limit of injection speed for which the RS has negative velocity. Assuming the jet cross section of the order of 1 pc, these injection speeds correspond to a jet kinetic luminosity of around $10^{45} \text{ erg s}^{-1}$. Interestingly this upper limit of injection speed depends on the composition parameter even for uniform cross-section jet. Our results indicate that in FR II jets typically with jet kinetic luminosities above $10^{46} \text{ erg s}^{-1}$, both FS and RS would move forward. On the other hand, in FR I jets with lower luminosities, either backwardly moving RS or RF could form. Hence, the numerical simulations of FR I jets need special care, partly because of it, but also because other processes including the entrainment of ambient material seems to become important (e. g., [Perucho & Martí 2007](#)).

DATA AVAILABILITY

The data underlying this article will be shared on reasonable request to the corresponding author.

ACKNOWLEDGMENTS

The work of DR was supported by the National Research Foundation (NRF) of Korea through grants

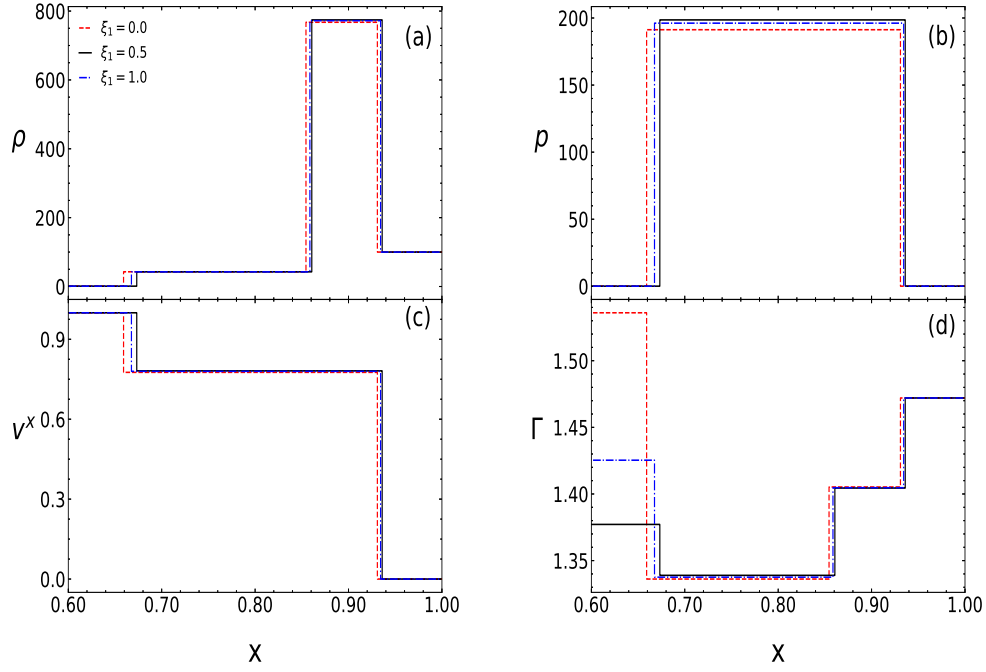


Figure 12. Flow variables ρ (a), p (b), v^x (c) and Γ (d) as functions of x at $t = 1.0$ for a jet beam with composition parameter $\xi_1 = 0.0$ (red dashed), $\xi_1 = 0.5$ (solid black), $\xi_1 = 1.0$ (blue dot-dashed). The composition parameter of ambient medium is taken to be $\xi_6 = 1.0$. The initial discontinuity is at $x_0 = 0.001$.

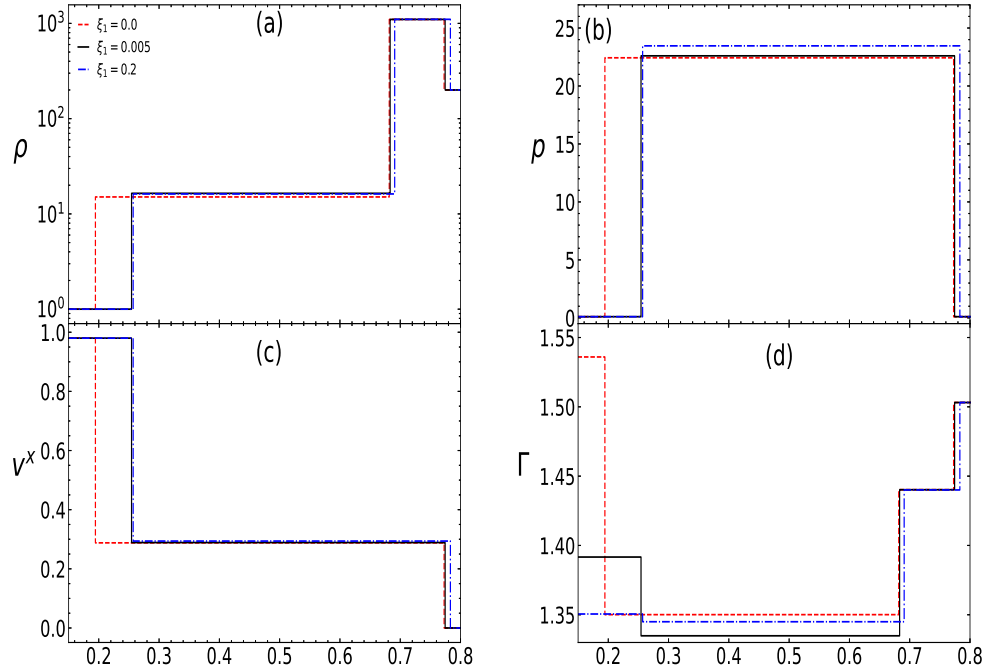


Figure 13. Flow variables ρ (a), p (b), v^x (c) and Γ (d) as functions of x at $t = 1.0$ for a jet beam with different composition parameters. The ambient medium consists of pure electron-proton plasma.

2016R1A5A1013277 and 2020R1A2C2102800. RKJ acknowledges Mr. Kuldeep Singh for help in python and cartoon diagram plotting.

REFERENCES

- Aloy M.-Á., Martí J.-M., Gómez J.-L., Agudo I., Müller E., Ibáñez J.-M., 2003, *ApJL*, 585, L109
 Arnett D., Fryxell B., Muller E., 1989, *ApJ*, 341, L63.
 Balsara D.S., 1994, *Journ. Comput. Phys.*, 114, 284
 Begelman M. C., Cioffi D. F., 1989, *ApJL*, 345, L21

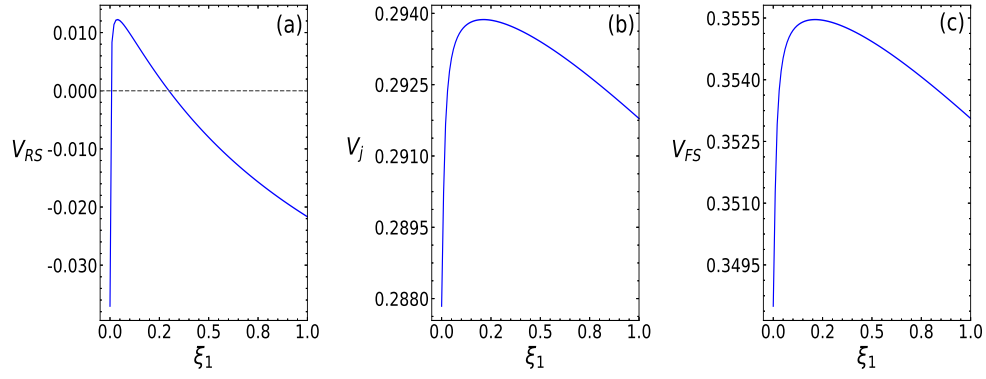


Figure 14. The propagation velocities of (a) the RS i. e., V_{RS} , (b) the CD i. e., V_j and (c) the FS i. e., V_{FS} are plotted as a function of ξ at $t = 1.0$ for a jet beam with different composition parameters. The ambient medium consists of pure electron-proton plasma. Initial conditions same as Fig. 13.

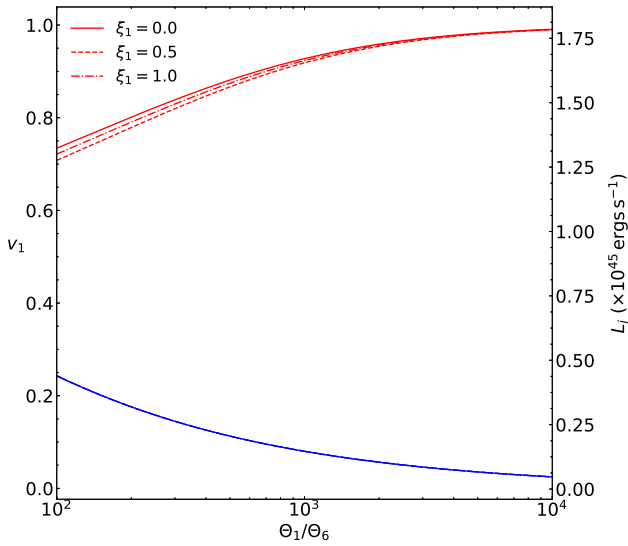


Figure 15. Injection speed v_1 (L_j) as a function of Θ_1/Θ_6 , for $\rho_1 = 1.0$, $p_1 = 1.0$ and $p_6 = 0.1$. The curves corresponds beam composition $\xi_1 = 0$ (solid), $\xi_1 = 0.5$ (dashed) and $\xi_1 = 1.0$ (dashed-dotted), while the composition of the ambient medium is $\xi_6 = 1.0$. The top curves (red) are upper value of v_1 (or L_j) for which the RS goes in the opposite direction to the JH and the bottom curves (blue and merged for all ξ_1) represent the upper limit of v_1 (or L_j) for which RF is formed instead of RS.

Blandford R. D., Rees M. J., 1974, MNRAS, 169, 395
 Chandrasekhar S., 1938, *An Introduction to the Study of Stellar Structure*. Dover, New York.
 Cox J. P., Giuli R. T., 1968, *Principles of Stellar Structure, Vol. 2*. Gordon and Breach Science Publishers, New York.
 Chattopadhyay I., Ryu D., 2009, ApJ, 694, 492
 Chattopadhyay I., Chakrabarti S. K., 2011, IJMPD, 20, 159
 Chattopadhyay I., Ryu D., Jang H., 2013, ASInc, 9, 13.
 Chattopadhyay I., Kumar R., 2016, MNRAS, 459, 3792
 Cielo S., et. al., 2014, MNRAS, 439, 2903.
 Curtis H. D., 1918, Lick Obs. Publ., 13, 31
 Dai W., Woodward, P. R., 1997, SIAM J. Si. Stat. Comput., 18, 982
 Dihingia I. K., Das S., Maity D., Chakrabarti S., 2018, PhRvD, 98, 083004

Dolezal A., Wong S. S. M., 1995, Journ. Comput. Phys., 120, 266
 Doeleman S. S., et al., 2012, Science, 338, 355
 Duncan G. C., Hughes P. A., 1994, ApJ, 436, L119
 Eulderink F., 1993, Numerical Relativistic Hydrodynamics, PhD Thesis, (Rijksuniversiteit te Leiden, Leiden, Netherlands)
 Eulderink F., Mellema G., 1995, A&AS, 110, 587
 Fender R. P., Gallo E., Russell D., 2010, MNRAS, 406, 1425
 Falle S. A. E. G., Komissarov S. S., 1996, MNRAS, 278, 586
 Gallo E., Fender R. P., Pooley G., 2003, MNRAS, 344, 60
 Harpole A., Hawke I., 2019, ApJ, 884, 110
 Junor W., Biretta J. A., Livio M., 1999, Nature, 401, 891
 Kamm, J. R. 2015 *An exact, compressible one-dimensional Riemann solver for General, convex equations of state*, Loss Alamos Report.
 Kim W. T., Ostriker E. C., 2001, ApJ, 559, 70.
 LeVeque R. J., 1992 *Numerical Methods for Conservation Laws*, 2nd edn., Birkhäuser.
 Lora-Clavijo F. D., Cruz-Perez J. P., Guzman F. S., Gonzalez J. A., 2013, Revista Mexicana de Fisica E, 59, 28.
 Marquina A., et. al., 1992 A& A, 258, 566,
 Marti J. M., Muller E., 1994, JFM, 258, 317
 Marti J. M., Muller R., 1994, Ibanez J. M., 1994, A&A, 281, L9
 Marti J. M., Müller E., Font J. A., Ibanez J. M. 1995, ApJ, 448, L105
 Marti J. M., Müller E., 1996, Journ. Comp. Phys., 123, 1
 Marti J. M., Müller E., 2003, LRR, 6, 7
 Marti J. M., Muller E., 2015, LRCA, 1, 3
 Matzner C. D., 2003, MNRAS, 345, 575
 Marscher A. P., Gear W. K., 1985, ApJ, 298, 114
 Martí J. M., Müller E., Font J. A., Ibáñez J. M. Z., Marquina A., 1997, ApJ, 479, 151
 Mignone A., Plewa T., Bodo G., 2005, ApJS, 160, 199
 Mizuta A., Yamada S., Takabe H., 2004, ApJ, 606, 804
 Pons J. A., Martí J. M., Müller E., 2000, JFM, 422, 125
 Rezzolla L., Zanotti O., 2001, JFM, 449, 395
 Roe P. L., 1981, Journ. Comput. Phys., 43, 357
 Rushton A., Spencer R., Fender R., Pooley G., 2010, A&A, 524, A29
 Ryu D., Ostriker J. P., Kang H., Cen R., 1993, ApJ, 414, 1
 Ryu D., Brown G. L., Ostriker J. P., Loeb A., 1995, ApJ, 452, 364
 Ryu D., Chakrabarti S. K., Molteni D., 1997, ApJ, 474, 378
 Ryu D., Chattopadhyay I., Choi E., 2006, ApJS, 166, 410
 Sarkar S., Chattopadhyay I., 2019, IJMPD, 28, 1950037
 Sarkar S., Chattopadhyay I., Laurent P., 2020, A&A, 642, A209
 Scheck L., et. al., 2002, MNRAS, 331, 615
 Sod G. A., 1978, JCoPh, 27, 1
 Singh K., Chattopadhyay I., 2019, MNRAS, 488, 5713.

- Syngé J. L., 1957, *The Relativistic Gas*. North Holland Publ. Co., Amsterdam.
- Taub A. H., 1948, PhRv, 74, 328
- Toro, E. 1997 *Riemann Solvers and Numerical Methods for Fluid Dynamics*. Springer.
- van Putten M. H. P. M., 1993, ApJ, 408, L21
- Vyas M. K., Kumar R., Mandal S., Chattopadhyay I., 2015, MNRAS, 453, 2992
- Vyas M. K., Chattopadhyay I., 2018, A&A, 614, A51
- Perucho M., Martí J. M., 2007, MNRAS, 382, 526
- Walg S., Achterberg A., Markoff S., Keppens R., Meliani Z., 2013, MNRAS, 433, 1453
- Wen L., Panaitescu A., Laguna P., 1997, ApJ, 486, 919
- Wilson J. R., 1972, ApJ, 173, 431

APPENDIX A: EXACT SOLUTION OF RIEMANN PROBLEM WITH CR EOS

Riemann problem is the time evolution of an initial discontinuity between two non-uniform states. Depending upon the initial conditions it can evolve into different combinations of rarefaction and shock waves and the possible scenarios are

- (i) Rarefaction-Contact-Shock (RCS)
- (ii) Shock-Contact-Shock (SCS)
- (iii) Rarefaction-Contact-Rarefaction (RCR)

Exact solutions of Riemann problem have been extensively used to test the accuracy of numerical simulation codes. Here, we present solutions for three type of Riemann problems, (i) RCS (as shown in Fig. 3b in the main text) which is known as the shock-tube test, (ii) SCS which is mathematical model of a situation when two fluids collide head on supersonically, and (iii) wall-shock (WS) problem which is physically equivalent to a supersonic flow which hits a wall. We also compare the analytical WS solution with that of a relativistic one-dimensional relativistic TVD code obtained by Ryu et. al. (2006); Chattopadhyay et. al. (2013). The solution to the Riemann problem is obtained by solving the jump condition across shock, and solving an ordinary differential equation arising out of self similarity condition of the rarefaction waves.

A1 RCS

The RCS problem has a rarefaction fan, a contact discontinuity and a forward shock.

A1.1 Shock front evaluation

The evolution of shock wave is governed by Rankine-Hugoniot jump conditions as described in section (2.2). The post shock velocities are obtained as

$$v_b^{y,z} = h_a \gamma_a v_a^{y,z} \left[\frac{1 - (v_b^x)^2}{h_b^2 + (h_a \gamma_a v_a^x)^2} \right]^{1/2} \quad (\text{A1})$$

Where subscript a (b) denotes the state ahead (behind) the shock and v^t is the absolute value of tangential velocity of the flow.

$$v^t = \sqrt{(v^y)^2 + (v^z)^2} \quad (\text{A2})$$

The normal component of “star state” velocity v_s^{x*} prior to the shock front is by equation (37).

$$v_s^{x*} = \frac{[h_a \gamma_a v_a^x + \gamma_s (p^* - p_a)/j]}{[h_a \gamma_a + (p^* - p_a) \{\gamma_s v_a^x / j + 1 / (\rho_a \gamma_a)\}]} \quad (\text{A3})$$

Here $*$ and a are the states behind and ahead to the shock front. For the right (left) shock, a will be the initial right (left) state. As from equation (28)

$$j = j(\rho_a, p_a, \rho^*, p^*) \quad (\text{A4})$$

we need the value of density in star state region ρ^* in order to calculate v_s^{x*} . This value of density can be calculated by solving the Taub adiabat (eq. 39) for ρ^* using any iterative root finder method (we have used bisection method) for a given value of p^* . Now we have to match this p^* and v_s^* with the starred pressure and velocity obtained from RF tail.

A1.2 Relativistic Rarefaction Waves

Rarefaction waves are represented by the self-similar solutions of the flow equations. All the quantities describing the fluid depend on the variable $\alpha = (x - x_0)/t$, where x_0 is the position of the interface separating the initial left and right states (see, Pons et. al. 2000, for details). Substitution of the derivatives of x and t in terms of derivative of α (equation 9) results in

$$(v^x - \alpha) \frac{d\rho}{d\alpha} + \{\rho \gamma^2 v^x (v^x - \alpha) + \rho\} \frac{dv^x}{d\alpha} + \rho \gamma^2 (v^x - \alpha) \left(v^y \frac{dv^y}{d\alpha} + v^z \frac{dv^z}{d\alpha} \right) = 0 \quad (\text{A5})$$

$$\rho h \gamma^2 (v^x - \alpha) \frac{dv^x}{d\alpha} + (1 - v^x \alpha) \frac{dp}{d\alpha} = 0 \quad (\text{A6})$$

$$\rho h \gamma^2 (v^x - \alpha) \frac{dv^y}{d\alpha} - v^y \alpha \frac{dp}{d\alpha} = 0 \quad (\text{A7})$$

$$\rho h \gamma^2 (v^x - \alpha) \frac{dv^z}{d\alpha} - v^z \alpha \frac{dp}{d\alpha} = 0 \quad (\text{A8})$$

From equation (A7) and (A8) we conclude that if there is no tangential velocity in the initial state, no tangential flow will develop inside the rarefaction. Since the process along α is isentropic

$$\frac{dp}{d\alpha} = h c_s^2 \frac{d\rho}{d\alpha} = \rho \frac{dh}{d\alpha} \quad (\text{A9})$$

The determinant of the system (A5)-(A8) vanishes for the non-trivial solution, and one obtains either $\alpha = \beta_1$ or $\alpha = \beta_5$ (see, equation 14). We are following the convention where the plus (minus) sign corresponds to the rarefaction wave propagating to right (left). We can reduce the system (A5)-(A8) to an ordinary differential equation (Marti & Müller 1994; Pons et. al. 2000)

$$\rho h \gamma^2 (v^x - \alpha) dv^x + (1 - \alpha v^x) dp = 0 \quad (\text{A10})$$

and two algebraic conditions

$$h \gamma v^y = \text{constant} \quad (\text{A11})$$

$$h \gamma v^z = \text{constant} \quad (\text{A12})$$

Equations (A11) and (A12) are similar to the equation (34) obtained for the shock. Hence the expression for the transverse velocity given in equation (A1) can also be used to calculate the transverse velocity components prior to the rarefaction waves.

Using the value of $\beta_{1,5}$ from equation (14), equation (A10) can be written in the form

$$\frac{dv^x}{dp} = \pm \frac{1}{\rho h \gamma^2 c_s} \frac{1}{\sqrt{1 + g(\alpha_{\pm}, v^x, v^t)}} \quad (\text{A13})$$

$$\frac{dv^x}{d\rho} = \pm \frac{c_s}{\rho \gamma^2} \frac{1}{\sqrt{1 + g(\alpha_{\pm}, v^x, v^t)}} \quad (\text{A14})$$

Where

$$g(\alpha_{\pm}, v^x, v^t) = \frac{(v^t)^2 (\alpha_{\pm}^2 - 1)}{(1 - \alpha_{\pm} v^x)^2} \quad (\text{A15})$$

We have considered $\alpha_- = \beta_1$ and $\alpha_+ = \beta_5$. The sign \pm corresponds to the sign taken in equation (14). Normal velocity prior to the rarefaction can be calculated by integrating the equation (A14). For ID or fixed Γ EoS, the method to find out the solution of the Riemann problem is relatively easy. The equation of motion describing the RF (equation A14) admits an analytical solution for ID EoS, and is known as the Riemann Invariant. And therefore, starting from the left state (region 1), we use the Riemann Invariant to obtain the flow variables in region 3. While we use the shock conditions to obtain the flow variables in region 4 in terms of those in region 6. Then equating velocity and pressure in region 3 and 4, we obtain a polynomial of the pressure. Solving which we reconstruct the full solution. However, for a general EoS, equation (A14) on integration does not admit an analytical solution. Therefore, the solution of Riemann problem is not trivial for general EoS like CR. In the following, we present the general method to solve the Riemann problem (see, Kamm 2015, for fluids with Newtonian equations of motion).

A1.3 Rarefaction Fan evaluation

For right going FS and left going RF (refer to Fig. 3b), it is clear that the tail of RF (region 2) is adjacent to the starred state (region 3) and the head adjoins the initial state (region 1). From Eq. (A9) we obtain the relation between ρ , p , and c_s ,

$$\frac{dp}{d\rho} = h(\rho, p) c_s^2 \quad (\text{A16})$$

To obtain the p^* starting from initial state of region 1, equation (A16) is numerically integrated from initial state with known pressure and density to the final star state with given p^* and unknown density ρ^* . The problem of determining the unknown star state density is addressed computationally by following the steps mentioned below,

(i) We solve the differential equation by RK-4 method for a constant density step size $\delta\rho$ for M number of integration steps such that

$$\bar{\rho}^* = \rho^M = \rho^{M-1} + \delta\rho \quad (\text{A17})$$

where $\bar{\rho}^*$ is the provisional value of star state density. As the correct value of $\delta\rho$ is unknown, consequently we do not know the correct value of ρ^* .

(ii) If $I(\delta\rho, \rho_a, p_a)$ be the value of pressure obtained by numerical integration then this value of pressure should be equal to p^* , as the pressure remains continuous across the contact.

$$p^* - I(\delta\rho, \rho_a, p_a) = 0 \quad (\text{A18})$$

We can calculate the actual step size by solving the equation (A18). Once the correct value of step size is known the normal component of the flow velocity adjacent to the tail is calculated by integrating the equation (A14)

$$(v_r^x)^* = v_a \pm \int_{\rho_a, p_a}^{\rho^*, p^*} \frac{c_s}{\rho \gamma^2} \frac{1}{\sqrt{1 + g(\alpha_{\pm}, v^x, v^t)}} d\rho \quad (\text{A19})$$

And the corresponding spatial location for the m^{th} integration step is given by

$$x^{(m)} = x_0 + \alpha_{\pm} (\rho^{(m)}, p^{(m)}, v^{(m)}) t \quad (\text{A20})$$

The final step of integration (M^{th} step) for equation (A20) corresponds to the position of tail. Here $\alpha_+ = \beta_5$ and $\alpha_- = \beta_1$ (from equation 14).

As the normal component of the flow velocity across the contact discontinuity is continuous

$$(v_r^{x*}) - (v_s^{x*}) = 0 \quad (\text{A21})$$

The value of ‘‘star state’’ pressure is obtained by solving equation (A21) by any iterative root finder method. Once p^* is computed the tangential velocity components can be calculated using equation (35) for shock wave and equations (A11, A12) for the rarefaction wave.

The solution of Riemann problem is given in table 1 and some of these solutions are shown in fig (A1). The existence of the upper limit of speed in relativity, causes various velocity components to be related to each other through the Lorentz factor, solutions depend strongly on the different combinations of initial v^t . For high values of v^t , the values of v^x are low. Therefore, solutions with $v^t = 0$ is faster and hotter than solutions with $v^t \neq 0$. The solutions from relativistic TVD codes proposed before (Ryu et. al. 2006; Chattopadhyay et. al. 2013) have been compared with these Riemann solutions and they agree well.

A2 Shock-Contact-Shock (SCS)

The collision of two streams is the physical scenario which can be associated with the shock-contact-shock (SCS) Riemann problem. Referring back to of Fig. 3a, SCS can be represented if regions 2 and 5 both are surfaces of the shock waves, instead of 2 being RF. Equation (A3) provides an expression for v_3^x in terms of v_1^x for a left moving shock and an expression for v_4^x in terms of v_6^x for a right moving shock.

$$v_3^x = \left(h_1 \gamma_1 v_1^x + \frac{\gamma_s (p_* - p_1)}{j} \right) \left(h_1 \gamma_1 + (p_* - p_1) \left(\frac{\gamma_s v_1^x}{j} + \frac{1}{\rho_1 \gamma_1} \right) \right)^{-1} \quad (\text{A22})$$

$$v_4^x = \left(h_6 \gamma_6 v_6^x + \frac{\gamma_s (p_* - p_6)}{j} \right) \left(h_6 \gamma_6 + (p_* - p_6) \left(\frac{\gamma_s v_6^x}{j} + \frac{1}{\rho_6 \gamma_6} \right) \right)^{-1} \quad (\text{A23})$$

v_1^t	v_6^t	p^*	v_*^x	ρ_3	ρ_4	v_3^t	v_4^t	V_s	x_H	x_t
0.000	0.000	1.49	0.66	1.22	4.80	0.0000	0.0000	0.78	0.36	0.54
0.000	0.900	2.91	0.47	2.00	6.34	0.0000	0.6422	0.60	0.36	0.47
0.000	0.990	5.64	0.23	3.27	8.32	0.0000	0.9141	0.33	0.36	0.41
0.900	0.000	0.41	0.34	0.48	2.53	0.9140	0.0000	0.55	0.43	0.55
0.900	0.900	0.98	0.28	0.89	3.98	0.9242	0.7997	0.40	0.43	0.53
0.900	0.990	2.91	0.17	2.00	6.34	0.9267	0.9501	0.24	0.43	0.49
0.990	0.000	0.17	0.13	0.25	1.45	0.9903	0.0000	0.39	0.48	0.52
0.990	0.900	0.29	0.11	0.38	2.08	0.9912	0.8753	0.24	0.48	0.51
0.990	0.990	0.92	0.09	0.86	3.87	0.9927	0.9779	0.14	0.48	0.50

Table A1. Solution of Shock tube problem at $t = 0.25$ in spatial domain $x \in [0, 1]$ with initial data $p_1 = 10.0$, $p_6 = 0.1$, $\rho_1 = 5.0$, $\rho_6 = 1.0$, $v_1^x = 0.0$, $v_6^x = 0.0$. The location of the initial discontinuity is at $x_0 = 0.5$, x_H and x_T are the positions of rarefaction head and tail respectively. In all cases we have taken composition parameter $\xi = 1.0$.

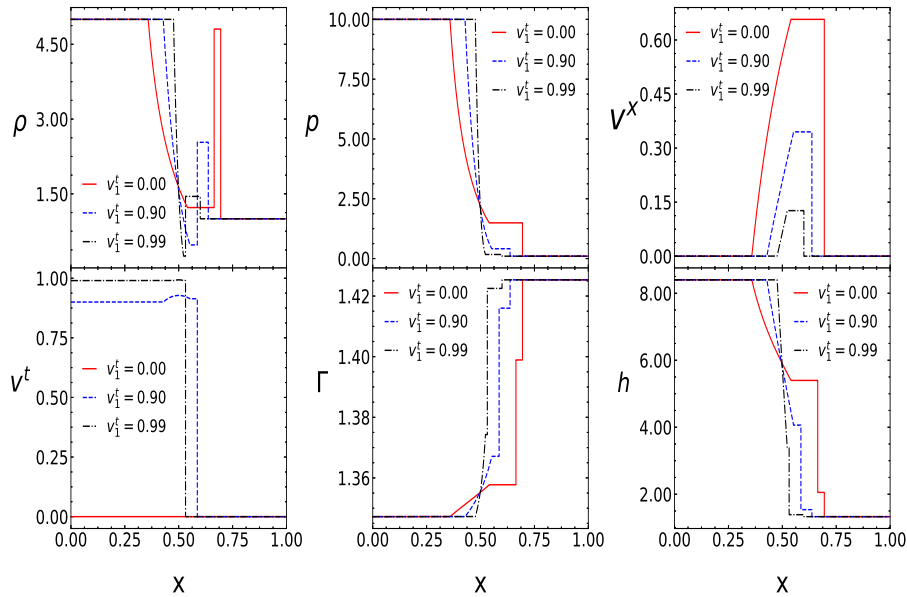


Figure A1. Comparison of ρ , p , v^x , v^t , Γ , and h , all plotted at the time $t = 0.25$. Initial conditions $\rho_1 = 5$, $\rho_6 = 1$, $p_1 = 10$, $p_6 = 0.1$, $v_1^x = v_6^x = 0.0$, $v_1^t = 0$ (solid, red), $v_1^t = 0.9$ (dashed, blue) and $v_1^t = 0.99$ (dash-dotted, black) and for all cases initial $v_6^t = 0$. The fluid composition is $\xi = 1.0$.

For equation (A22) j is the negative root of equation (28) and for equation (A23) it is the positive root of equation (28). Across the contact discontinuity

$$v_3^x - v_4^x = 0 \quad (\text{A24})$$

Equation (A24) is solved for p^* using the iterative root finder and rest of the quantities can be calculated once p^* is obtained. Densities in region 3 and 4 are obtained from the Taub's adiabat for left and right shock respectively. The solution (ρ , p , v^x , v^t , Γ , & h) is presented in Fig. (A2a-f) for two time snap $t = 0.25$ (solid, dashed) and $t = 0.5$ (dashed, blue). It is clear that both the shocks are moving apart from each other and the shock velocity is actually in the direction

opposite to the local flow velocities v^x . The initial condition used for this particular model is

$$\begin{aligned} \rho_1 = 10.0, \quad p_1 = 10, \quad v_1^x = 0.5, \quad v_1^t = 0.2; \quad \text{and} \\ \rho_6 = 10.0, \quad p_6 = 10.0, \quad v_6^x = -0.5, \quad v_6^t = 0. \end{aligned} \quad (\text{A25})$$

The two shock surfaces are at the either side of $x = x_0$, and the CD is marked by the jump in v^t .

A3 Solution of relativistic wall shock problem

The relativistic wall shock problem is a mathematical model of the collision between a fluid of density ρ_1 moving with extremely high velocity v_1 (presently along right) and a reflecting wall. The fluid after being reflected back, gets compressed

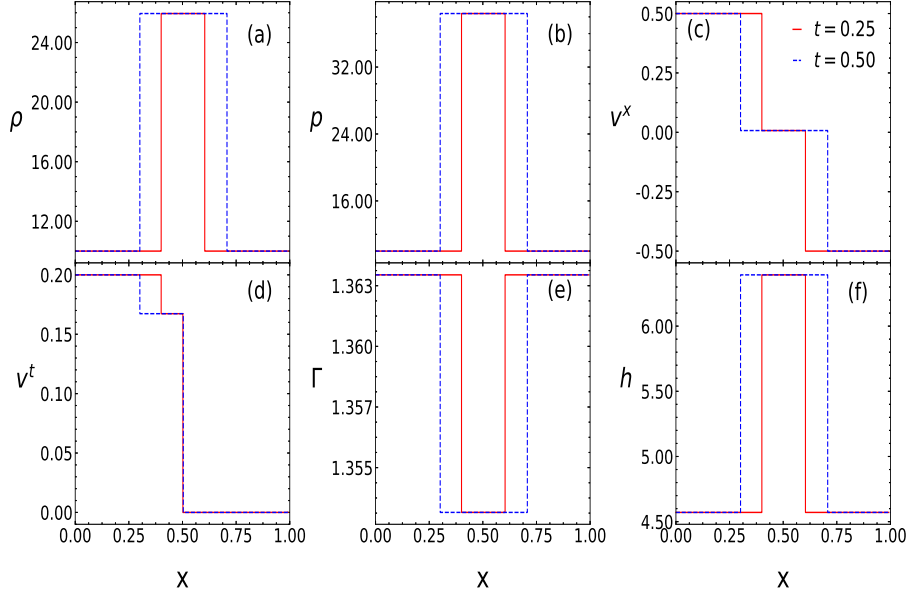


Figure A2. SCS: Flow variables (a) ρ , (b) p , (c) v^x , (d) v^t , (e) Γ and (f) h as a function of x , for Shock-Contact-Shock case at $t = 0.25$ and for fluid composition $\xi = 1.0$.

and eventually a reverse shock is generated. The shock moves in the opposite direction of the fluid leaving behind a hot and compressed fluid with zero velocity in post shock region. The fluid density, pressure and velocity of fluid in post shock region are represented by ρ_2 , p_2 and v_2^x respectively. As velocity in post shock region $v_2^x = 0$, we need only two equations to find out ρ_2 and p_2 . We can use equations (37) and (39) to find out the post shock density and pressure. From equation (37) we have

$$h_1 \gamma_1 v_1^x + \frac{\gamma_s (p_2 - p_1)}{j} = 0 \quad (\text{A26})$$

As shock is moving towards the left direction j should be taken as negative root of equation (28)

$$j = - \left(- \frac{(p_1 - p_2)}{(h_1/\rho_1 - h_2/\rho_2)} \right)^{1/2} \quad (\text{A27})$$

From equation (39)

$$h_1^2 - h_2^2 = \left(\frac{h_1}{\rho_1} + \frac{h_2}{\rho_2} \right) (p_1 - p_2) \quad (\text{A28})$$

We can solve the equations (A26) and (A28) using the Newton-Raphson method to obtain ρ_2 and p_2 . The shock velocity is calculated using (38)

$$V_s = \frac{\rho_1^2 \gamma_1^2 v_1 - |j| \sqrt{j^2 + \rho_1^2 \gamma_1^2 (1 - v_1^2)}}{\rho_1^2 \gamma_1^2 + j^2} \quad (\text{A29})$$

If x_0 is the location of wall then the shock location after time t is given by

$$x_s = x_0 + V_s t \quad (\text{A30})$$

In Fig. A3a-c, we plot the flow variables ρ , p , and v^x as a function of x . The solid red lines show the exact solutions and the solutions marked by black open circles are obtained using relativistic TVD code of Chattopadhyay et. al. (2013). The initial conditions for this problem are

$$\rho_1 = 1.0, \quad p_1 = 1.0, \quad \text{and} \quad v_1^x = 0.8 \quad (\text{A31})$$

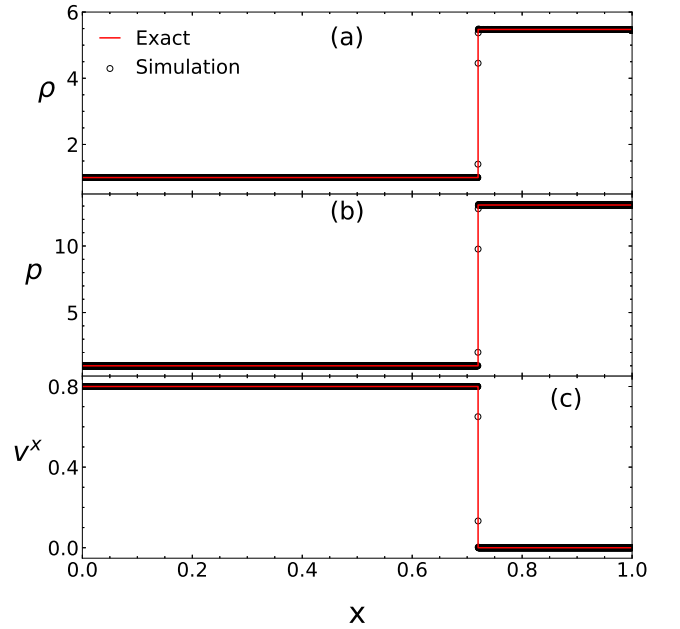


Figure A3. WS: Solution of the wall shock problem with initial condition $\rho_1 = 1.0$, $p_1 = 1.0$, and $v_1 = 0.8$. The solution is obtained for wall located at $x_0 = 1.0$, composition parameter $\xi = 0.5$ and $t = 0.8$.

The solution contains only one discontinuity in the form of a shock jump, across which ρ , p and v^x are discontinuous.

This paper has been typeset from a $\text{\TeX}/\text{\LaTeX}$ file prepared by the author.